FRACTURE CHARACTERIZATION FROM ATTENUATION AND GENERATION OF TUBE WAVES

by

E.L. Hardin, C.H. Cheng, F.L. Paillet[1], and J.D. Mendelson

Earth Resources Laboratory
Department of Earth, Atmospheric, and Planetary Sciences
Massachusetts Institute of Technology
Cambridge, MA 02139

ABSTRACT

Results are presented from experiments carried out in conjunction with the USGS at the Hubbard Brook Experimental Forest near Mirror Lake, New Hampshire. The study focuses on our ability to obtain orientation and transmissivity estimates of naturally occuring fractures. The collected dataset includes a four-offset hydrophone vertical seismic profile, full waveform acoustic logs at 5, 15 and 35 kHz, borehole televiewer, temperature, resistivity, and SP logs, and well-to-well pump test data. While the basic assumptions of the VSP generation model are found to be tenable, fracture aperture estimates from VSP were generally one order of magnitude lower than corresponding pump test or Stoneley wave attenuation results. A new model for tube wave generation which makes use of fracture stiffnes (stress/length) is presented.

INTRODUCTION

The importance of fractures in site characterization and resource recovery has created interest in methods of evaluating the significance and basic properties of distributed fractures from borehole observations. This study is mainly involved with seismic responses from the full waveform acoustic logging tool and hydrophone vertical seismic profile. We begin by applying the tube wave generation model of Beydoun et al. (1985), and the FWAL Stoneley attenuation model of Mathieu (1984) to the same fractures in the same well. Based on this comparison, additional realism is incorporated into the VSP model, which improves agreement between fracture parameters estimated from FWAL and VSP.

The data set consists of standard wireline logs, FWAL and hydrophone VSP from a research well in crystalline rock near Mirror Lake, New Hampshire. Seismic interpretation is compared to independent estimates of fracture parameters from hydrologic

[1]USGS, Denver, CO 80225

pump tests and borehole televiewer images. The objective is to calibrate the seismic techniques to flow test results, and to improve our understanding of the interactions which result in the observable seismic responses. The parallel plate analogy is used throughout as a basis for considering the mechanical and flow behavior of fractures, even though there are indications of limited usefulness for this model.

Hydrophone VSP and FWAL Seismic Experiments

The hydrophone VSP apparatus and survey methods are thoroughly described in Hardin and Toksöz (1985). In short, hydrophones in a borehole streamer register both the direct compressional wave from a remote source (which couples to the fluid), and tube waves which may also be excited. In crystalline rock studies (Huang and Hunter, 1982; Beydoun et al. 1985) there is good correlation between fracture type and density, and horizons where tube waves are generated concurrently with the direct arrival.

The FWAL data reported here were acquired by the USGS Borehole Geophysics Research Project (Paillet, 1985), using variations of the Simplec tool. Different separation/spacing and different types of transmitters were used (Figures 1, 2 and 3). Attenuation of all the recognizable modes was typically observed at depths where borehole televiewer, electrical and/or flowmeter logs indicated fractures. In the boreholes studied, the seismic experiments did not respond to the majority but were selective of particular fractures.

Field Data and Site Description

Mirror Lake site well EBR-4 was percussively drilled to a depth of 225 m. The hole is one of a 10 m square pattern of similar holes (Figure 4) which penetrate a metamorphic sequence of schist and gneiss, intruded by thick, irregular veins of quartz monzonite (Winters, 1984). All four of the holes are uncased except for a 15 m surface layer of sand, gravel and till. Four shotholes are drilled and cased in the surrounding surface layer to a depth of 9 m. Thickness of the glacial drift varies, so that some of the shotpoints lie on or just above the bedrock contact. The level of standing water in each shothole corresponds approximately to published water table depth data (Winters, 1984). The horizontal distance from the observation well to each shot point is of the same order as the total depth of the well (Figure 5).

For the hydrophone VSP survey in EBR-4, a near-source geophone was used to monitor detonation timing and source signature. A total of four VSP sections were acquired, which is one more than the minimum needed to obtain distinct fracture parameters from inversion of the tube wave generation models of equations (A12) and (1). In each section the dominant events are tube waves which originate at about 44 m and propagate both upward and downward. In addition, smaller amplitude tube waves originating at 220

m, 135 m and 103 m are observed, and the direct compressional arrival is evident.

Conventional Logs

At the Mirror Lake site, the four EBR wells were logged using caliper, single-point resistivity, natural gamma, borehole televiewer and uncompensated sonic tools (Paillet, 1985). In addition nearby wells EBR-1, 2 and 3 were logged for self-potential (SP), focused resistivity, short and long normal resistivity, and neutron porosity (Winters, 1984). Televiewer images show an abundance of subhorizontal fractures from the surface down to about 100 m, where fracture traces become more sparse. Fracture indications tend to be clustered, with relatively consistent orientation within such assemblages. Dip angles range up to about 40 degrees. The majority of fractures in EBR-4 dip to the east, although some dip south and a few dip toward the west (Paillet, 1985).

The logs of Figures 6 and 7 clearly show the existence of fractures. Electrical responses suggest the presence of flow or clay minerals. Mineral alteration is naturally associated with discontinuities, gouge formation, and the chemical activity of groundwater. A useful correlation between mineralization (electrical response) and hydraulic significance does not generally follow (Paillet, 1985). To summarize the evaluation of conventional logs, fracture responses are clearly evident, but it is difficult to distinguish the VSP tube wave generating horizons or the features which are important in simple pump tests. These failures are probably related since in well EBR-4 inflow anomalies were associated with VSP tube wave generation. This is an important result of this study.

For adjacent wells EBR-3 and 4 it is interesting to note the correlation of electrical logs (SP, focused resistivity and single-point resistivity) with indications of fractures in EBR-4 from televiewer and hydrophone VSP (Figures 6,7 and 8–11). SP response is generally flat in the fractured zones, indicating that ionic concentration is relatively uniform within the borehole and the connecting fracture network. Significant electrochemical activity, and steady fluid exchange (flow) are therefore absent in these zones (Serra, 1984, p.79). The single-point resistance is affected by mineralization which may be associated with fractures. Clay minerals can provide cations for current conduction in resistive formations even when connate waters are fresh. Significant anomalies are seen at the larger fractures, indicating the presence of altered minerals. Extent of alteration does not necessarily correlate to transmissivity (Paillet, 1985).

Resistivity decreases sharply to 500 ohm-m or less at negative peaks which are well correlated to particular fractures. The peaks at 38 m, 44 m and 54 m are of possible importance in the investigation of VSP tube wave generation processes. Sharpness of resistivity anomalies at fractures increases with the resolution of the log, further indicating that the peaks are fracture-related.

Natural gamma response is dominated by intrusive features, with slight activity that may be associated with fracturing. Gamma activity in the intrusive veins is so variable that fracture responses are indiscernible. Realigning the gamma logs from the four EBR wells, it is possible to produce good correlation for lithology changes, but without elucidating fracture trends (Paillet, 1985).

INTERPRETIVE MODELS

Mechanistic models for understanding seismic responses are based on the parallel plate fracture analogy. The VSP tube wave generation model involves dynamic fracture closure, which expels fluid into the borehole producing tube waves. The FWAL Stoneley attenuation model also involves fluid transfer between a single fracture and the borehole, but with the parallel plate aperture fixed and fluid storage in the fracture due to compressibility only. This section gives a brief recapitulation of the published models, with underlying assumptions. Methods for applying the models to field data are described, and fracture parameters are calculated for significant features in well EBR-4.

Tube Wave Generation in VSP Surveys

White (1983) showed that a tube wave may be generated when an incident plane compressional wave interacts with the borehole at a contact between formations. Tube wave amplitude is predicted for the case of perpendicular borehole-interface geometry using a long-wavelength assumption and approximate displacement continuity conditions at the contact. In the data presented here, and in the surveys of Huang and Hunter (1981) and others, tube waves are typically generated at horizons which are distinguished only by fracture traces in an otherwise homogeneous formation. For body wave energy to be converted to tube waves at these thin features requires interaction in the form of fluid exchange between the formation and the borehole.

Tube Wave Generation VSP Model, Displacement Formulation

In the derivation of Beydoun et al. (1985), fractures are idealized as having parallel walls, being fluid-saturated and embedded in an isotropic elastic medium (Figure 12). The fracture-borehole system is initially at hydrostatic equilibrium. An incident P wave causes fracture width to oscillate around the static aperture at the same frequency and displacement amplitude as the incident wave. For the normal incidence, low frequency case this condition applies everywhere on the model fracture; this is referred to hereafter as the displacement formulation. To simplify calculation of fluid injection into the borehole the following assumptions are made:

1. Static fracture aperture is much larger than dynamic closure.
2. Only laminar fluid flow takes place in the fracture.
3. Fluid compressibility is negligible.
4. Fluid injected into the fracture does not significantly change the borehole fluid pressure.
5. The low frequency approximation with frequency dependence holds (i.e., the P wavelength is much larger than borehole radius or fracture width).
6. Fracture intrinsic permeability is invariant with time.
7. Closure varies sinusoidally; real-valued linear fracture response for application of spectral methods of data amplitude comparison.

For the two-dimensional case, laminar incompressible flow in response to induced pressure is given by Darcy's law. Fluid flow velocity is proportional to the hydraulic head gradient and conductivity. The model is derived initially for a hypothetical two-dimensional fracture (infinite in the third dimension) that abuts a fluid half-space (borehole). As is common in reservoir problems (Ziegler, 1976), calculation of 2-D flow is simplified with the assumption of an effective distance from the borehole boundary at which fracture flow is nil. Effective 2-D length is used as a limit of integration in the determination of total flow. It is convenient to define this distance arbitrarily in terms of aperture, frequency and fluid properties so that the pressure gradient is diminished to about a tenth of its maximum. The volume of fluid ejected from the fracture into the borehole is obtained by integrating the fluid conservation equation along the effective fracture length (Beydoun et al., 1985).

The two-dimensional result is adapted to the axisymmetric 3-D problem by comparing the 2-D and 3-D expressions for steady-state flow in response to constant pressure at the effective length. The conversion is purely geometrical and independent of frequency or fluid properties. For the conversion to be exact (in the context of an effective distance) requires that the pressure gradient be constant in the 2-D case.

Most of the strain energy of a propagating tube wave is trapped in the fluid, so the amplitude of a tube wave excited by a periodic dilatant source in the fluid may be approximated by equating the source strength to the dilatancy associated with the coherent tube wave. Neglecting phase response, body waves radiated into the solid, and associated energy of the normal mode in the solid, Beydoun et al. (1985) develop a relationship between fluid flow and tube wave pressure amplitude. Upgoing and downgoing tube waves of equal amplitude are predicted.

The tube wave dilatation in the fluid determines the amplitude of the tube wave generated by ejected fluid. The transfer of energy from the compressional body wave to the normal mode is taken as real-valued and linear with respect to frequency. The

integral of volume strain over one half-cycle is equated to the fluid volume ejected from the fracture in the same time period. The volumetric strain and amplitude are determined using the displacement potential for tube waves.

To determine *in situ* permeability the observed tube wave amplitude is normalized by the pressure amplitude of the direct compressional phase at the same sensor. The pressure in the borehole from the direct P wave is expressed in terms of the formation displacement amplitude, associated with a plane wave of arbitrary wavenumber (White, 1983). The normalized tube wave pressure amplitude, or tube:P spectral amplitude ratio, is then

$$\frac{p^t}{p^\alpha} = C(L_0)\frac{\omega\beta^2\cos(\phi)[1-(c\cos(\vartheta)/\alpha)^2]I_0(nR)}{\varsigma_0\cos(\vartheta)c^2\alpha[1-2(\beta\cos(\vartheta)/\alpha)^2]} \tag{1}$$

The amplitude of P wave displacement in the formation is thus eliminated by cancellation. The ratio of tube wave to compressional wave amplitude can be determined from a single trace if necessary and does not require hydrophone calibration. The two phases must be represented by recognizable wavelets and be correctable for interference from extraneous phases for the spectral ratio comparison to be meaningful.

Linear Inversion of VSP Generation Model for Fracture Orientation

For fixed frequency and fixed survey geometry, the tube wave vs. P wave spectral amplitude ratio (equation 1) in terms of fracture parameters is:

$$\frac{p^t}{p^\alpha} = B(L_0)\cos(\phi) \tag{2}$$

where $B(L_0)$ is a nonlinear function of equivalent flow aperture, borehole radius, formation properties, and fluid properties. Function $B(L_0)$ is the tube:P amplitude ratio for zero-offset, normal incidence geometry. For fixed survey geometry, ϕ is a function of fracture strike and dip, which are designated ψ and σ.

Borehole pressure is discretely sampled in the time domain, windowed to isolate the direct P wave and tube wave events, and transformed using the discrete Fourier transform (FFT), so that the spectral ratio at discrete frequencies is available for comparison to theory. Multiple VSP offsets are needed to utilize the geometrical dependence of spectral amplitude ratio for fracture orientation estimation.

With three or more offsets, at a fixed frequency, linear least squares inversion may be used to obtain fracture-normal vector direction cosines, leaving an undetermined transmissivity-dependent factor common to all offsets. The problem is represented as

$$\begin{bmatrix} (p^t/p^\alpha)_1 \\ (p^t/p^\alpha)_2 \\ \vdots \end{bmatrix} = \begin{bmatrix} p_{1,x} & p_{1,y} & p_{1,z} \\ p_{2,x} & p_{2,y} & p_{2,z} \\ \vdots & \vdots & \vdots \end{bmatrix} \begin{bmatrix} n_x \\ n_y \\ n_z \end{bmatrix} B(L_0) \tag{3}$$

where

$$B(L_0) = C(L_0)\frac{\omega\beta^2[1-(c\cos(\vartheta)/\alpha)^2]I_0(nR)}{\varsigma_0\cos(\vartheta)c^2\alpha[1-2(\beta\cos(\vartheta)/\alpha)^2]} \tag{4}$$

and $C(L_0)$ is given by Beydoun et al (1985). Parameters $p_{i,x}, p_{i,y}, p_{i,z}$ are components of the wavenumber vector $\mathbf{p}$ corresponding to the ith shot point. Similarly, n_x, n_y, n_z are the components of unit fracture normal $\mathbf{n}$.

Nonlinear Inversion of VSP Generation Model

Where source frequency content and data quality permit acquisition of reliable spectral ratio information over a frequency band, a different inversion approach is potentially useful. This method for obtaining fracture parameters was presented originally in Hardin and Toksöz (1985), and consists of finding a solution vector $\mathbf{x} = (L_0, \psi, \sigma)$ which results in a 'best fit' of the model to the processed data at a number of discrete frequencies over the entire source band. Nonlinear least squares (Marquardt) inversion is used to match theoretical spectral ratio curves with those obtained from pressure waveforms. The method seeks to exploit frequency dependence of the 'observed' tube:P amplitude ratio, which may be sensitive to fracture orientation.

The transmissivity (equivalent aperture) and orientation dependent parts of the Beydoun model are separable for a fixed frequency. The nonlinear approach is comparable to co-solving many linear inverse problems at the same time using the generalized inverse. Marquardt inversion with numerical derivatives was used originally because of flexibility in the programming; the behavior of the forward problem was investigated in the vicinity of the solution and found to be minimal.

Analysis of Well EBR-4, Mirror Lake, New Hampshire

Source spectra are studied by temporally windowing the arriving compressional wavelet at several receivers, and computing their spectra via the discrete Fourier transform (FFT). The spectra are normalized and combined to produce a composite amplitude spectrum for each section. Based on evaluation of the source spectra the traces are bandpass filtered between frequencies of 100 and 300 Hz.

A tube wave event is defined as a disturbance originating at a particular depth, concurrent with the direct compressional arrival, and travelling up- or down-hole from this depth. Each tube wave event is evaluated independently, using traces from the three filtered VSP sections. For each trace the arriving P wavelet and the selected tube wave event are windowed, and the tube:compressional amplitude ratio spectrum calculated. A spreading correction is made to each P wavelet spectrum, based on the difference between source-receiver separation for the recording hydrophone and the direct path

from the source to the generating fracture. These distances are known from directional surveys.

The inversion methods of the previous sections are applied to the tube wave generating horizons at 44 m and 225 m, yielding the results presented in Table 1. The amplitude ratios used in the linear inversion correspond to a peak source-band frequency of 150 Hz. Dip angles of these fractures are small (<10 degrees), and the direct paths from the shotpoints impinge on the upper fracture with shallow incidence. For these reasons the calculated strike angles vary considerably between linear and nonlinear methods, and televiewer indications. The upper range of the source band is reduced relative to a previous experiment (Hardin and Toksöz, 1985) because the shotpoints are located in the surface layer. Transmissivity values for linear and nonlinear methods are comparable.

STONELEY WAVE ATTENUATION IN FULL WAVEFORM LOGS

FWAL waveforms used in this study were acquired using a two-receiver, single transmitter tool with various geometry and transducer configurations. When an open fracture intervenes between receivers, significant amplitude diminution of all recognizable phases is observed at the farther receiver (Figure 13). Fracture attenuation of the Stoneley phase is best understood because the energy of this mode is largely trapped in the borehole fluid. Amplitude at typical FWAL frequencies can be approximated by the fluid pressure amplitude anywhere in the borehole. At a fracture opening the pressure amplitude is limited by fluid flow into the formation. The amplitude of the tube wave transmitted to the far receiver is thus related to fracture transmissivity. This effect forms the basis of calculating fracture transmissivity from FWAL response.

Head waves and pseudo-Rayleigh modes are also apparently attenuated from thru-fracture transmission. Much of the energy of these modes is elastic, and is scattered away from the borehole at intervening fractures. Apparent attenuation of these modes is probably dependent on the realism of the parallel-plate fracture analogy. Conversely, induced fracture flow, by which transmissivity effects are observable, should be relatively insensitive to realism of the assumed fracture geometry.

FWAL Stoneley Wave Attenuation Model

In the attenuation model of Mathieu (1984) the borehole is a long fluid-filled cylindrical cavity in an infinite elastic solid. The fracture-borehole system is saturated, and fluid flow in the fracture obeys Darcy's law. When a tube wave travels past the fracture, a portion of the propagating strain energy is lost to fluid flow. Incident energy is also scattered as transmitted and reflected tube waves as depicted in Figure 13. Pressure

continuity requires that at any point in the borehole, pressure contributions from incident and scattered tube waves are equivalent. Using the tube wave pressure function from Cheng and Toksöz (1981) it is clear that fluid pressure amplitude increases toward the borewall. Pressure amplitude of the transmitted tube wave is taken as limited by and equal to the pressure at the borewall which is 'seen' by the fracture. This is a reasonable approximation since tube wave pressure varies by no more than 10-20% over the borehole cross section. Fracture opening pressure and transmitted tube wave pressure are thus equal at the borewall. By averaging the flow associated with tube wave particle velocity over the cross sectional area of the borehole, and averaging fracture flow over the aperture at the borewall, mass conservation may be imposed to obtain an approximate flow balance at the fracture horizon at any moment in time. Thus if $\langle v \rangle$ represents particle velocity averaged over flow area, and S_B, S_F are the flow areas of the borehole and fracture openings, then

$$S_B \langle v_I \rangle = S_B \langle v_R \rangle + S_B \langle v_T \rangle + S_F \langle v_F \rangle \tag{5}$$

Characterizing the fracture response by Darcy's law, this balance equation provides the basis for deducing equivalent parallel-plate fracture aperture from comparison of P_I and P_T. The FWAL tool can be used to obtain only relative pressure P_T/P_I, by comparing pressure signal amplitude with and without an intervening fracture. None of the velocities (flow rates) in the conservation equation are measurable, and so it is necessary to invoke the concept of acoustic impedance to obtain an equivalent parallel-plate fracture aperture. Impedance is defined as

$$Z = \frac{\langle P \rangle}{\langle v \rangle} \tag{6}$$

where $\langle P \rangle$ is fluid pressure averaged over flow area. Impedance Z_B for borehole tube wave propagation, and impedance Z_F for flow in a parallel plate fracture system can be readily calculated (see Mathieu, 1984). The measurable pressure ratio for a single intervening fracture can then be expressed

$$\frac{P_T}{P_I} = \frac{P_F}{P_I} = \frac{Z_{FvF}}{Z_{BvI}} = \frac{1}{1+X} \tag{7}$$

where

$$X = \frac{nL_0}{2} \frac{I_0(nR)}{I_1(nR)} \frac{Z_B}{Z_F} \tag{8}$$

$$Z_B = c\rho_f \,, \qquad Z_F = \left\{ \frac{L_0^2}{12\mu} \left[\frac{1}{2R} + \frac{2}{\pi} \left(\frac{\omega}{b} \right)^{1/2} \right] \right\}^{-1} \tag{9}$$

This relationship is compared with observed fractional attenuation to determine an appropriate value for transmissivity $\rho g L_0^3/12\mu$. Calculated fractional attenuation is plotted against aperture in Figure 14, using geometry and formation parameters appropriate for well EBR-4.

Application of FWAL Attenuation Model

The effect of a significant fracture is such that phase changes occur within the Stoneley packet in addition to amplitude diminution. The spectral ratio method is useful for comparing the complex attenuation process with a real-valued model. A similar application was the estimation of intrinsic formation attenuation in FWAL, from spectral analysis of the head waves and pseudo-Rayeigh modes (Willis, 1983). An important outcome of this work is that when using waveforms from different transmitter-receiver pairs to characterize attenuation of a particular phase, stability is improved with a constant length window shifted to the arrival of the phase at each receiver.

This is the approach used in the investigation of Stoneley attenuation. For multiple receiver FWAL data, Stoneley phase amplitude is compared at the near and far receivers. Since formation properties vary only slightly exclusive of fractures in the crystalline sections considered, FWAL Stoneley velocity is fixed at about 95% of the borehole fluid velocity (clear water). The invariant window length is determined so as to include only the packet arriving at the Stoneley wave delay.

The ratio of far:near amplitude is determined in the form of a ratio spectrum. In the results presented here, a Hamming (1977) window is applied to the constituent time windows. To calculate a log of pressure ratio vs. depth it is desirable to reduce the ratio spectrum at each depth to a single representative value. Since the FWAL attenuation model is minimally dependent on frequency (Mathieu, 1984), it is reasonable to average the ratio spectrum over the frequency band where the incident tube wave has significant amplitude.

When signals from near and far receivers are compared for an unfractured interval in a homogeneous formation, a pressure ratio of unity should result. This is not often the case, because FWAL receiver gain is uncalibrated. To prevent receiver gain or bias from producing a baseline transmissivity response, observed pressure ratio is corrected by a factor derived from the pressure ratio in a known unfractured interval or casing.

Structural features of the borehole and the formation adjacent to the hole produce variability in FWAL waveforms. Changes in borehole diameter can scatter tube wave energy, creating secondary tube waves and radiating body waves (Stephen et al., 1985). Changes in the elastic properties of the formation can produce reflections (Paternoster, 1985), and reduce transmission (Bhasavanija, 1983) which may be interpreted as apparent attenuation. Also important is the stability of the spectral ratio method when a fracture intervenes between the transmitter and the near receiver. When this occurs both near and far waveforms are attenuated and the spectral ratio method may be vulnerable to noise or extraneous phases. Calculated transmissivity seems most reasonble where fracture spacing is on the order of the source-receiver separation and not much less. Extremal points calculated for densely fracture zones, and just below highly attenuating features, are probably erroneous. Significant features in the calculated logs

consist of several points over a small depth interval which is greater than the receiver spacing of the tool.

FWAL Stoneley Wave Attenuation Analysis, Well EBR-4

Three different FWAL tools were deployed in well EBR-4: resonant-source tools with characteristic frequencies of 34 and 15 kHz, and a sparker source tool which operates at about 5 kHz. A comparison of fracture transmissivity calculated for each type on a fractured interval is presented in Figure 15. For these calculations a single fracture is assumed to intervene between the two receivers. Transmissivity calculated from the higher frequency tools responds more impulsively at or near fractures than the transmissivity at 5 kHz (sparker source). The Stoneley packet is contaminated by pseudo-Rayleigh energy at the higher frequencies, so these responses are probably due in part to body wave scattering at fractures or other defects of the borewall. Transmissivity calculated for sparker data is less localized but correlates better with televiewer and pump test fracture indications.

DISCUSSION

Fracture parameters calculated using the published models are summarized in Table 2. A discrepancy exists between transmissivity derived from FWAL Stoneley attenuation and from VSP tube wave generation. Stoneley attenuation is sensitive to fractures which are open near the borehole. Conversely, the VSP response is evidently produced at those fractures which are in hydraulic communication and are capacious for some distance, say a wavelength, away from the borehole. Both models are approximate since simplifying assumptions must be made to avoid excess parameterization. It will be shown below that the FWAL model is in much better agreement with flow test and televiewer data than the VSP model. An explanation for the discrepancy is presented in the next section in the form of a VSP tube wave generation model which utilizes stress equilibrium across a fracture with intrinsic stiffness.

Plane Fracture Orientation

For well EBR-4 the agreement between inversion and televiewer orientation is not good. Three factors contribute jointly to this apparent lack of agreement. Firstly, the direct paths from the shot points to the upper depths were shallow, resulting in degraded data quality. Second, because of the shallow depth of the shotholes, surface and near surface reflections complicate the uppermost waveforms. Perhaps most importantly, however, televiewer images indicate that fractures at Mirror Lake are not simple tabular features;

the images rather suggest discrete but complex networks of flow paths. This result may seriously hinder the determination of flow orientations from televiewer images.

Pump Testing at Mirror Lake Well EBR-4

A constant-discharge pump test was performed on two successive days immediately prior to the VSP experiment (Paillet, personal communication). While water was pumped from well EBR-4, the levels of wells EBR-1, 2 and 3 were monitored. In addition a sensitive flowmeter was used in EBR-1, 2 and 3 to determine the depths where outflow (and inflow) occurred. Hydraulic communication was produced between the peripheral wells and EBR-4 by pumping, and the path of communication was defined by flow measurement (Figure 4). Water level changes in the peripheral wells were used during the test to establish that steady flow conditions were achieved. The levels in EBR-1, 2 and 3 fell at a fairly constant rate from the start, as 7.6 liters/minute were discharged from EBR-4 (Figure 16). Water loss from storage in all four boreholes constituted about 30% of the total discharge from pumping. Water level in the four wells fell virtually in unison throughout the test.

A wireline flowmeter operating on a heat-pulse, mass flow principle (Hess, 1982) was deployed successively in the four wells. The tool was positioned at a fixed depth in the hole and axial fluid velocity in the borehole measured repeatedly. Flow measurements at different depths were used to locate discrete inflow/outflow horizons to within one meter.

To the accuracy of the tool (about 5% of total discharge), all of the inflow to EBR-4 entered at 44 meters. This depth corresponds exactly to an indication of a major fracture in the VSP analysis, to within the accuracy of depth measurement (0.3 m). The FWAL and televiewer logs indicate fracturing here and elsewhere in the well.

Outflow from EBR-1, 2 and 3 was also isolated to single, discrete fractures in each well. If fracture orientation from televiewer logs is extrapolated away from each well to the other wells, it becomes apparent that the flow paths connnecting EBR-1, 2 and 3 with EBR-4 do not follow any identifiable planar fracture. Either there is communication between different sets of subparallel fractures, or the major fracture is not planar. This observation is difficult to reconcile with the parallel-plate fracture analogy.

Inflow was observed in EBR-2, about 4 meters below the outflow horizon. The two depths correspond to similar televiewer indications of parallel fractures. During the test the level in EBR-2 was lower than that of EBR-1 and 3, so inflow to EBR-2 is strong evidence for indirect flow paths between the four wells.

Transmissivity between the wells was evaluated using a formula for a couplet of wells connected by a single, infinite parallel-plate fracture (Paillet, personal communication).

Considering the fracture as a thin porous layer, transmissivity was calculated between pairs of wells consisting of EBR-4 and EBR-1, 2 or 3. The results vary between 0.3 cm^2/sec and 2.3 cm^2/sec and are given in Table 3. These are approximate since only well couplets are considered, and actual flow paths between the wells are probably indirect.

Intrinsic Fracture Stiffness

For the two tube wave generating horizons for which independent estimates are available, transmissivity calculated from the VSP tube wave generation response is significantly smaller than that deduced from direct flow observation. Moreover, the FWAL attenuation model predicts transmissivity values which are comparable in magnitude to the flow test data. It is reasonable then to consider how the VSP model departs from realism and what are the impacts on calculated transmissivity.

A realistic, *in situ* fracture transmits the static forces of overburden, Poisson-effects caused by changing load conditions and finite rigidity, and tectonic forces. A significant portion of the stress-bearing performance of a saturated fracture system may come from fluid pressure (effective stress), but equilibrium is maintained by bridging of irregularities in the fracture walls. Natural conditions may exist where fracture opening support is derived from excessive fluid pressure or large pressure gradients, but these are local effects which only change the scale length of bridging by asperities.

In the displacement formulation (1) the incident P wave displacement amplitude is taken as the assumed amplitude of fracture closure. If the fracture stiffness (resistance to normal closure) were close to that of the formation, closure would be small since the fracture width is much less than a wavelength. Conversely, if the fracture offered little resistance to closure it would behave much like a free surface: closure would be about twice the P wave displacement and there would be no transmitted P wave. Examination of field data shows little diminution of transmitted amplitude (Figures 8–11). The fracture closure assumption is a compromise, tending to underestimate permeability since the closure amplitude associated with observed transmissivity is smaller than the P wave displacement.

The variability of bridging in any direction may be expressed as the characteristic scale length or distance between points of contact. To develop an asperity contact model for comparison to the displacement formulation, it is helpful to recognize that the scale length is much smaller than a wavelength at exploration frequencies. Fracture deformability can then be simplified to a relation between perpendicular compressive stress and fracture closure. For seismic processes no detectable 'set' is imparted to a fracture by the passage of a seismic wave, and elastic behavior is assumed. If linear behavior is also assumed, then fracture deformability is specified by a single parameter: intrinsic stiffness (or its inverse compliance). Such a model is equivalent to a thin layer

of finite thickness, which is more deformable and permeable than the intact mass.

Derivation of (observable) tube:compressional wave pressure ratio using intrinsic stiffness κ begins with a relationship of fracture aperture to external stress and internal pressure:

$$L(s,t) = (P_f(s,t) - P_n(t))/\kappa \tag{10}$$

where P_f is the transient fluid pressure in the fracture associated with the incident normal stress P_n. The incident normal stress is uniform everywhere on the fracture, and the static equilibrium imposed by (10) ensures that it is uniform across the fracture as well. By contrast, in the displacement formulation fracture closure is assumed uniform everywhere.

The incident stress is easily found for an incident plane wave travelling along an arbitrary axis x' with harmonic displacement. Axial and transverse normal stresses are simply

$$u(x',t) = \varsigma_0 e^{i(\omega t + kx')} \tag{11}$$

$$P_{x',x'} = i\rho\omega\varsigma_o\alpha e^{i(\omega t + kx')} \tag{12}$$

$$P_{y',y'} = P_{z',z'} = i\rho\omega\varsigma_o \frac{(\alpha^2 - 2\beta^2)}{\alpha} e^{i(\omega t + kx')} \tag{13}$$

If the arbitrary axis x' forms an included angle of ϕ with the fracture normal, then the normal stress on the fracture is derived from Mohr's circle:

$$P_n = \frac{P_{x',x'} + P_{z',z'}}{2} + \frac{P_{x',x'} - P_{z',z'}}{2}\cos 2\phi = i\omega P_\varsigma e^{i\omega t} \tag{14}$$

Substitution yields the following expressions for aperture and its time derivative:

$$L(s,t) = L_0 + \frac{(P_f(s,t) - i\omega P_\varsigma e^{i\omega t})}{\kappa} \tag{15}$$

$$\frac{\partial L}{\partial t} = \frac{1}{\kappa}\left(\frac{\partial P_f}{\partial t} + \frac{\omega^2 P_\varsigma}{\kappa} e^{i\omega t}\right) \tag{16}$$

If the amplitude ς_0 of transient closure is much smaller than the static aperture ($|L(s,t) - L_0| << L_0$) then to a good approximation the static aperture may be used in flow calculations. A description of 1-D steady fracture flow is found in the 'cubic law' (Snow, 1965)

$$q(s,t) = -\frac{L_0^3}{12\mu}\frac{\partial P_f}{\partial t}, \qquad \frac{\partial q}{\partial s} = -\frac{L_0^3}{12\mu}\frac{\partial^2 P_f}{\partial s^2} \tag{17}$$

Following the displacement formulation, the continuity equation is used to relate inflow, displacement and storage of fluid in a volume element of fracture fluid:

$$-dqdt = \frac{dL}{dt}dsdt + L(s,t)\gamma\frac{dP_f}{dt}dsdt\,. \tag{18}$$

Rearranging and switching to partial derivatives (functions $L(s,t)$ and $P(s,t)$ are both separable in independent variable s and t) gives

$$-\frac{\partial q(s,t)}{\partial s} = \frac{\partial L(s,t)}{\partial t} + L(s,t)\gamma\frac{dP_f(s,t)}{dt} \tag{19}$$

Substituting (15) and (16) the following nonlinear equation is found:

$$\frac{\partial^2 P_f}{\partial s^2} = \frac{\partial P_f}{\partial t}\left\{D_1 + D_2 e^{i\omega t}\right\} + D_3 P_f \frac{\partial P_f}{\partial t} + D_4 e^{i\omega t} \tag{20}$$

$$D_1 = \frac{12\mu}{L_0^3}\left\{\frac{1}{\kappa} + \gamma L_0\right\}, \qquad D_2 = -i\frac{12\mu\omega\gamma P_{\zeta_o}}{L_0^3\kappa} \tag{21}$$

$$D_3 = \frac{12\mu\gamma}{L_0^3\kappa}, \qquad D_4 = \frac{12\mu\omega^2 P_{\zeta_o}}{L_0^3\kappa^2} \tag{22}$$

Whereas (20) is nonlinear, the relative importance of linear and nonlinear terms depends on the coefficients D_1, $D_2, \ldots$. By assigning realistic values to formation and fluid properties, and reasonable bounds to the pressure behavior, the coefficients for the second and third terms of the right hand side are shown to be relatively small (Appendix A). The approximate linear equation is

$$\frac{\partial^2 P_f}{\partial s^2} = D_1\frac{\partial P_f}{\partial t} + D_4 e^{i\omega t} \tag{23}$$

The boundary conditions applicable to the analytical solution are $P_f(0,t) = 0$, and finite pressure at arbitrarily large s. The resulting solution (Appendix A) is

$$P_f(s,t) = \frac{iD_4}{\omega D_1}\left(1 - e^{\left\{-s\sqrt{\frac{\omega D_1}{2}}(1+i)\right\}}\right)e^{i\omega t} \tag{24}$$

A linear approximation is used to relate the readily obtained 2-D solution (24) to realistic 3-D geometry. Pressure P_f is approximated by a linear function on the interval $s = [0, d]$ so that the resulting 2-D ejected volume V_{2D} is easily converted to the necessary V_{3D}. The ratio of compressional:tube wave pressure ratio can then be obtained in the same manner as the displacement formulation (Appendix A). This ratio is plotted for various values of stiffness in Figure 17 using normal incidence, zero-offset geometry.

Pressure ratio increases between the water-layer and virtual-layer stiffness bounds. For stiff fractures pressure ratio is reduced because the fracture is held open by asperity contact. As stiffness becomes very small the effective radius $S_{10\%}$ does also, reducing borehole pressure 'amplification' due to cylindrical geometry, which in turn reduces the generated tube wave amplitude. This behavior can be seen in Figure 18, where 2-D pressure is plotted against distance s from the 'borehole' boundary. For decreasing

stiffness, the 2-D pressure attains larger amplitude, but closer to the borehole. For unrealistic stiffness values far below the equivalent water-layer bound (by a factor of 4 or more), pressure ratio p^t/p^α actually decreases due to this effect.

If equivalent parallel-plate flow aperture is assigned to static aperture L_0, then the appropriate stiffness may be found by matching the 'observed' pressure ratios to the model (Figure 17). For the fracture at 44 m, the average flow aperture from all tests is 0.55 mm. Stiffness values appropriate for each offset at 150 Hz (source band center frequency) vary between 2.6×10^{12} to 1.2×10^{13} (MPa/meter). The corresponding equivalent water layer, and virtual-layer stiffness values are 3.6×10^{12} and 3.5×10^{14} MPa/m, respectively. The following observations are based on application of this model to Mirror Lake VSP data:

1. Calculated stiffness values lie near the low end of the expected range, and one of the values is smaller than the equivalent water-layer value.
2. Stiffness values for the fracture at 44 m, and the four source offsets, differ by a little less than one order of magnitude. The expected range is two orders.
3. Frequency dependence of the pressure model is greater than that of the ratio spectra derived from data.

Intrinsic stiffness evidently contributes to the forces which resist closure, imparting roughly as much stiffness as an undrained water layer with thickness equal to the parallel-plate flow aperture. If intrinsic stiffness is to be characterized by a thin layer, the layer compressibility may actually be far less than water. This is because the mechnical aperture is several times greater than the flow aperture. It is known from *in situ* experiments in jointed crystalline rock that mechanical aperture (from direct measurement of fracture displacement) is typically several times larger than equivalent parallel-plate flow aperture (Voegele et al., 1981). The difference is attributed to flow path tortuosity. In the compressible layer model, compressibility must increase with increasing thickness to attain the same stiffness. In this context the low stiffness values calculated for EBR-4 represent the ratio of real aperture (larger than flow aperture) to equivalent layer compressibility which is significantly greater than that of water.

CONCLUSIONS

The results of the analysis of the hydrophone VSP, FWAL and flow data at Mirror Lake can be summarized as follows:

1. The borehole televiewer, FWAL Stoneley attenuation and hydrophone VSP responses are characteristic of different fracture properties. The televiewer records the

trace of every fracture and in addition to location, can provide a qualitative indication of weathering and structural significance. FWAL Stoneley attenuation occurs at only a few of the fractures detected by the televiewer, and is always associated with such a fracture (when the borewall is otherwise smooth and impermeable). The FWAL responds to near-field features which may be damaged by drilling, in addition to features which are major fluid conduits. In the EBR-4 survey the VSP response occurs only at hydraulically significant features, probably because of greater depth of investigation. Significance was determined by flow testing which can be a costly method for sampling heavily fractured formations.

2. The displacement formulation of the VSP tube wave generation model underestimates transmissivity by about one order of magnitude. This was observed in EBR-4 with reliable independent transmissivity estimates. The reason is probably the assumption for amplitude of fracture closure. The stress formulation provides transmissivity values which are in agreement with the pump test and FWAL results, but requires *a priori* knowledge of fracture stiffness.

3. As a first approximation, fracture stiffness of hydraulically significant features is of the same order as an undrained fluid layer with thickness equal to the flow aperture. Additional field data sets which include pump test results are needed to improve this generalization. Shear zones or seams filled with soft, relatively impermeable clay-like material may actually have stiffness which is much smaller than expected from the flow aperture. This behavior would result in overestimated transmissivity, but might be predicted from televiewer images showing very large apertures.

4. The basic assumptions underlying the VSP generation model are supported by agreement with field results. Frequency dependence in the source band is comparable to that observed. Evidence that incident energy couples to the fracture fluid through normal stress or displacement coupling at the fracture walls is given by the agreement of calculated orientation and the flow paths for pump test measurements. Orientation calculations are more successful with a broadband source discharged well within the bedrock, reducing the surface reflection and surface layer reverberation, and improving accuracy of recorded frequency dependence of p^t/p^α.

5. Wells EBR-1,2,3 and 4 provided a good opportunity to correlate structural characterization and transmissivity determinations between three adjacent boreholes. Structural expressions deduced from televiewer images could not be correlated between holes spaced 10 m apart, which simply confirms that fracture continuity cannot be estimated from single-borehole observations. Individual fractures can be observed in the thin fracture zone at 44 m in EBR-4, which exhibit orientations quite different from the zone at large. Orientation deduced from VSP tube wave generation is more consistent with that inferred for the zone. Transmissivity measured under steady flow conditions at the same horizon varied by a factor of 2 between different pairs of wells. Inflow observed in one of the observation wells during constant discharge from EBR-4 is strongly suggestive of channel flow. Quantitative work in such a heterogeneous medium requires close

attention to the characteristic scale of measurement, and the relation of the affected region to the rock mass.

APPENDIX

VSP Generation Model, Stress Formulation Linear Approximation

To compare magnitudes of the various terms of the right hand side of (20), known values for α, β, ρ, γ, ϕ, and ω are adopted, and the magnitudes of the derivatives are estimated. If the strain amplitude of the incident wave is taken as 10^{-6}, then the displacement amplitude is known to be $A = (\alpha/\omega) \cdot 10^{-6}$, and P_ζ is determined. The magnitude of the fluid pressure is limited to the incident stress magnitude $|P(s,t)| \leq \omega P_\zeta$. The time derivative of the fluid pressure is approximated by the maximum time derivative of the incident pressure:

$$\left|\frac{\partial P_f}{\partial t}\right| \approx \omega^2 P_\zeta$$

Stiffness for a fracture of specified aperture is bounded approximately by the behavior of an equivalent layer of water, and a layer of intact rock ('virtual' layer). For the undrained fluid case stiffness is $\kappa = k/L_0$, where k is dynamic bulk modulus. In the virtual fracture case stiffness is the ratio of stress to integrated strain or $\kappa = \rho\alpha^2/L_0$.

Taking the magnitude of the fourth term $D_4 e^{i\omega t}$ as unity, the terms of the right hand side are compared in Table A1. The estimated magnitudes of the second and third terms are equivalent and are more than four orders of magnitude smaller than the remaining terms. This result is independent of fracture stiffness. Based on the 10^4 difference in magnitude, the second and third (nonlinear) terms of (20) are dropped from the model. Errors in magnitude estimates for the dropped terms, due to approximations used for P_f and $(\partial P_f)/(\partial t)$, are assumed to be much less than 10^4. The linearized model then takes the tractable form

$$\frac{\partial^2 P_f}{\partial s^2} = \frac{\partial P_f}{\partial t} + D_4 e^{i\omega t} \tag{A1}$$

with analytical solution

$$P_f(s,t) = A_1 e^{A_2 t + A3t} + \frac{A_4}{\omega} e^{i\omega t} + A_5 s + A_6 \tag{A2}$$

Substituting into (A1) yields the conditions

$$A_4 = \frac{iD_4}{D_1}, \qquad A_3 = \pm\sqrt{D_1 A_2} \tag{A3}$$

If $P(s,t)$ is to be finite at large s or t, then it is clear that $A_5 = 0$, $A_3 = -\sqrt{D_1 A_2}$, and A_2, A_3 are complex with magnitudes no greater than unity. At large s the pressure reduces to

$$P_f(s \to \infty, t) = \frac{iD_4}{\omega D_1} + A_6 = \frac{i\omega P_\zeta}{1 + \kappa\gamma L_0} e^{i\omega t} + A_6 \tag{A4}$$

At the borewall the condition $P(0,t) = 0$ is applied as in the displacement formulation, which yields

$$P(0,t) = A_1 e^{Re\{A_2\}t(\cos Im\{A_2\}t + i \sin Im\{A_2\}t)} + \frac{iD_4}{\omega D_1} e^{i\omega t} + A_6 \,. \tag{A5}$$

Equating like terms yields

$$A_1 = -\frac{iD_4}{\omega D_1} \,, \qquad A_6 = 0 \tag{A6}$$

$$P(s,t) = \frac{iD_4}{\omega D_1} \left(1 - e^{\left\{ -s\sqrt{\frac{\omega D_1}{2}}(1+i) \right\}} \right) e^{i\omega t} \tag{A7}$$

$$P_\zeta = \rho \zeta_o \left(\alpha - \frac{\beta^2}{\alpha} (1 - 2\cos\phi) \right) \tag{A8}$$

Pressure amplitude of the generated tube wave may be calculated in the same manner as the displacement formulation (Beydoun et al., 1985) if the 2-D pressure function is first linearized. This approach, while approximate, circumvents solution of the linearized but nonseparable partial differential equation in cylindrical coordinates.

The distance $s_{10}\%$ from the borehole at which the pressure gradient magnitude decays to 10% of its value at the borewall, is determined analytically:

$$\left| \frac{\partial p(s_{10\%})}{\partial s} \right| = 10\% \left| \frac{\partial p(0)}{\partial s} \right| \,, \qquad s_{10\%} = \ln\left\{ \frac{1}{10\%} \right\} \sqrt{\frac{2}{\omega D_1}} \tag{A9}$$

Variation of the 2-D pressure in the interval $[0, s_{10\%}]$ must be approximated as a linear function in order to apply the 2-D result to fracture flow in 3-D. A plot of complex pressure function P_f with time dependence $e^{i\omega t}$ removed is shown for a frequency of 200 Hz (Figure 19). The dominant imaginary component is in-phase with the normal stress field incident on the fracture. The integral of pressure magnitude on $s = [0, s_{10\%}]$ represents the dominant behavior and can be used to obtain the linear approximation:

$$P_f(s,t) \approx sP^*(t) \,, \qquad P^* = \frac{2}{s_{10\%}} \int_0^{s_{10\%}} |P_f(s,t)| \, ds \tag{A10}$$

The volume ejected from the 2-D fracture during a half-cycle of fracture closure is corrected to 3-D radial flow, and equated to the integrated dilatation for one half-cycle of a tube wave at the same frequency. Tube wave amplitude factor C is thus determined in terms of the amplitude of particle motion for the plane wave incident on the fracture. This is an upper bound on the amplitude of the generated wave, since fluid dilatation is conserved. Ejected 2-D volume is

$$V_{2D} = \frac{L_0^3 P^*}{12\mu s_{10\%}} \int_0^{\pi/\omega} \sin\omega t dt = \frac{L_0^3 P^*}{6\mu\omega s_{10\%}} \tag{A11}$$

The correction to radial geometry follows the displacement formulation exactly. Using (10) and (11)

$$V_{3D} = 2\pi R \chi V_{2D} \tag{A12}$$

with the same definitions for χ and d. Tube wave amplitude factor C is then

$$C = \frac{nV_{3D}}{4\pi Rk(2 - c^2/\alpha_f^2) I_1(nR)} \tag{A13}$$

Pressure amplitude of the direct compressional wave at the borehole sensor was determined by White (1983, p.149). Following the displacement formulation the tube:compressional wave pressure amplitude ratio takes the form

$$\frac{p^t}{p^\alpha} = \frac{(\rho_f c^2 C I_0(nR))(\beta^2(1 - \{\frac{c}{\alpha}\cos\vartheta\})^2)}{\omega\alpha\rho_f c^2(1 - 2\left\{\frac{\beta}{\alpha}\cos\vartheta\right\}^2)} \tag{A14}$$

NOTATION

α, β, ρ	formation P wave velocity, S wave velocity, density
α_f, ρ_f	borehole fluid P wave velocity, density
R	borehole radius
μ, γ	borehole fluid dynamic viscosity (Pa-sec) and compressibility (Pa^{-1})
ζ_0	amplitude of P-wave displacement in the formation
$u(t)$	P-wave displacement in the direction of propagation
n	fracture unit normal vector
p	incident P wavenumber unit vector
b	borehole unit direction vector, oriented downward
ϕ	included angle between P wavenumber and fracture normal
θ	included angle between P wavenumber and borehole axis
ψ, σ	fracture strike and dip angles
$L(s,t)$	fracture aperture, as a function of 2-D distance s from the 'borehole' boundary, and time
L_0	equivalent parallel-plate flow aperture (average over time)
K	fracture permeability ($Length^2$)
K_c	fracture hydraulic conductivity (Length/Time)
T	fracture transmissivity ($Length^2$/Time)
$h(s,t)$	hydraulic head for 2-D fracture, as a function of distance s from the 'borehole' boundary
$H(s,t)$	2-D fracture pressure
V_{2D}, V_{3D}	volume of fluid ejected into the borehole, for the 2-D and 3-D cases
q_{2D}, q_{3D}	rate of fluid flow into the borehole, for the 2-D and 3-D cases
v_{avg}	average 2-D fracture flow velocity
$F(\omega, \zeta_0/L_0)$	integral proportional to fluid displacement during one half-cycle of fracture wall displacement
$d(L_0)$	effective radius of fracture
$\chi(L_0)$	geometrical conversion factor for converting 2-D to 3-D flow into the borehole
$C(L_0)$	proportionality factor for the dependence of the displacement potential for the generated tube wave on the fracture closure
p_α, p_t	borehole fluid pressure amplitude for the incident P wave and generated tube wave, respectively.
$c(\omega)$	tube wave phase velocity

k	$= \omega/c$ tube wave axial wavenumber
n	$= k(1 - c^2/\alpha_f^2)^{1/2}$ tube wave radial wavenumber from the fluid compressional wave contribution
Φ_f^T	tube wave fluid displacement potential
Δ_f^T	tube wave fluid dilatation
I_0, I_1	Modified Bessel functions of the first kind
$B(L_0)$	tube:P wave pressure ratio for zero offset, normal incidence geometry
$\mathbf{x}$	aperture, strike, dip fracture parameter solution vector
λ	factor containing orientation dependence of (VSP) displacement model
$\mathbf{A}$	aperture dependence of (VSP) displacement model
$\mathbf{G}$	nonlinear functional representing (VSP) displacement model
$\mathbf{d}$	vector containing spectral ratio observations, for a particular source offset
$\mathbf{W}$	diagonal matrix of weights applied to spectral ratio residuals
$\mathbf{f}$	objective function for nonlinear (VSP) model inversion
J_n	numerical Jacobian of objective function $\mathbf{f}$
D_n, α_n	Levenberg-Marquardt inversion parameters
$\mathbf{s}$	unit vector in direction of solution vector $\mathbf{x}$
P_I, P_R ,P_T	tube wave pressure incident on, reflected from, and transmitted through fracture
P_F	transient pressure at fracture opening in borewall
$P(r,z,t)$	tube wave pressure field
v_I , v_R, v_T	tube wave particle velocity incident on, reflected from and transmitted through fracture
v_F	flow velocity at fracture opening in borewall
S_B	borehole cross-sectional area
S_F	cross-sectional area of fracture opening in borewall
Z_B	borehole tube wave impedance
Z_F	fracture flow impedance
P_ζ	constant containing orientation and formation properties dependence on pressure due to incident plane wave
P_f	transient fracture fluid pressure due to incident wave
κ	fracture stiffness (Stress/Length)
$D_1 \ldots D_4$	coefficients in (VSP) stress model

REFERENCES

Beydoun, W.B., C.H.Cheng and M.N.Toksöz, 1985, Detection of open fractures with vertical seismic profiling: J. Geophys. Res., 90, 4557-4566.

Bhashvanija, K., 1983, A Finite Difference Model of an Acoustic Logging Tool: The borehole in a horizontally layered geologic medium: Ph.D. Thesis (T-2763), Colorado School of Mines.

Biot, M.A., 1952, Propagation of elastic waves in a cylindrical bore containing a fluid: J. App. Phys., 23, 997-1005.

Bower, D.R., 1983, Bedrock fracture parameters from the interrpetation of well tides: J. Geophys. Res., 88, 5025-5035.

Brown, K.M., 1972, Computer Oriented Methods ofr fitting tabular data in the linear and nonlinear least squares sense: Department of Computer, Information, and Control Sciences, TR No. 72-13, Univ. of Minnesota.

Cheng, C.H. and M.N.Toksöz, 1981, Elastic wave propagation in a fluid filled borehole and synthetic acoustic logs: Geophysics, 46, 1042-1053.

Cheng, C.H., M.N.Toksöz and M.E.Willis, 1982, Determination of in situ attenuation from full waveform acoustic logs: J. Geophys. Res., 87, 5477-5484.

Cheng, C.H. and M.N.Toksöz, 1983, Determination of shear velocities in 'slow' formations: Trans., 24th Ann. SPWLA Symp., Calgary, Alberta, Canada.

Hamming, R.W., 1977, Digital Filters: Prentice-Hall Signal Proc. Series, A.V. Oppenheimer, ed., Prentice-Hall, Inc., N.J.

Hess, A.E., 1982, A heat-pulse flowmeter for measuring low velocities in boreholes: U.S. Geol. Survey Open-File Report 82-699, 40p.

Huang, C.F. and J.A.Hunter, 1981, The correlation of "tube wave" events with open fractures in fluid filled boreholes: Current Research, Part A, Geological Survey of Canada, Paper 81-1A, 361-376.

Marquardt, D.W., 1963, An algorithm for least squares estimation of nonlinear parameters: SIAM J. Appl. Math., 11, (2).

Mathieu, F., 1984, Application of full waveform acoustic logging data to the estimation of reservoir permeability: S.M. Thesis, Mass. Institute of Technology.

Paillet, F.L., 1980, Acoustic propagation in the vicinity of fractures which intersect a fluid filled borehole: Trans. 21st Ann. SPWLA Symp., Lafayette, Louisiana.

Paillet, F.L., 1983, Frequency and scale effects in the optimization of acoustic waveform logs: Trans. 24th Ann. SPWLA Symp., Calgary, Alberta, Canada.

Paillet, F., 1985, Geophysical well log data for study of water flow in fractures near Mirror Lake, New Hampshire: U.S. Geol. Survey Open-File Report 85-340.

Paternoster, B., 1985, Effects of layer boundaries on full waveform acoustic logs: S.M. Thesis, Mass. Institute of Technology.

Schoenberg, M., 1980, Elastic wave behavior across linear slip interfaces: J. Acoustical Soc. Am., 68, 1516.

Schoenberg, M., T.Marzetta, J.Aron and R.P.Porter, 1981, Space-time dependence of acoustic waves in a borehole: J. Acoustical Soc. Am., 70, 1496.

Serra, O., 1984, Fundamentals of Well Log Interpretation: 1. The Acquisition of Data: Elsevier, 423 p.

Snow, D.T., 1965, A parallel plate model of fractured permeability media: Ph.D. Thesis, University of California, Berkeley.

Stephen, R., F. Pardo-Casas and C.H. Cheng, 1985, Finite-difference synthetic acoustic logs: Geophysics, 50, 1588-1609.

Stewart, R.R., R.M.Turpening and M.N.Toksöz, 1981, Study of a subsurface fracture zone by vertical seismic profiling: Geophys. Res. Letters, 8, 1132-1135.

Voegele, M.D., E.L.Hardin, R. Lingle, M. Board, N. Barton, 1981, Site characterization of joint permeability using the heated block test: Proc. 22nd U.S. Symp. Rock Mechanics, Mass. Institute of Tech. Center for Adv. Engr. Study.

White, J.E., 1983, Underground Sound, Elsevier, 252 p.

Willis, M.E., 1983, Seismic velocity and attenuation from full waveform acoustic logs: Ph.D. Thesis, Mass. Institute of Technology.

Winters, T., 1983, Geohydrologic setting of Mirror Lake, West Thornton, New Hampshire: U.S. Geol. Survey Water Resources Investigations Report 84-4266.

Ziegler, T.W., 1976, Determination of rock mass permeability: U.S. Army Corps of Engineers, Waterways Experiment Station, Tech.Report S-76-2.

Well Name	Frac Depth (m)	Linear Inversion			Nonlinear Inversion		
		Strike	Dip	T (cm^2/s)	Strike	Dip	T (cm^2/s)
MIRROR LAKE	44	N60E	8S	2e-4	N23W	21W	2e-4
WELL EBR-4	225	N54E	11S	5e-6	N1E	13E	4e-6

Table 1: VSP Tube Wave Generation Analysis Using Displacement Formulation (Beydoun et al., 1985) with Linear and Nonlinear Inversion Methods.

WELL NAME, DEPTH	Parameter	Televiewer	FWAL Attenuation (5 kHz)	VSP Inversion (nonlinear)	Independent estimate
MIRROR LAKE 44 m.	T (cm^2/s) Strike Dip	N110E 10S	1.2	2e-4 N25W 20W	≈ 1.0
MIRROR LAKE 225 m.	T (cm^2/s) Strike Dip	N60E 15S	0.1	4e-6 NS 15E	

Table 2: Summary of fracture parameters determined from televiewer images, FWAL Stoneley attenuation, VSP model inversion, and independent transmissivity estimates. At Mirror Lake a constant-discharge pump test was performed (see text). Transmissivity was calculated from FWAL data, using Stoneley attenuation in data acquired with a sparker source tool operating at approximately 5 kHz, Figure 12).

Infinite Flat Fracture of Uniform Aperture, Borehole Couplet

Obs. Well	Well Separation (m)	Head Diff. (m)	Flow Rate Range (l/min)	T (cm^2/s)	Equiv. Aperture (mm)
EBR-1	13	1.2	2.3	2.3	0.8
			1.1	1.1	0.7
EBR-2	10	3.9	2.3	0.65	0.5
			1.1	0.3	0.4
EBR-3	10	1.1	0.8	0.7	0.5
			0.4	0.35	0.4

Equivalent Cylindrical Conduit (Tube) of Tortuosity = 2

Obs. Well	Well Separation (m)	Head Diff. (m)	Flow Rate Range (l/min)	Tube Aperture (mm)
EBR-1	13	1.2	2.3	5.2
			1.1	4.3
EBR-2	10	3.9	2.3	3.6
			1.1	3.0
EBR-3	10	1.1	0.8	3.7
			0.4	3.1

Table 3: Pump Test Analysis, Mirror Lake Well EBR-4 (after Paillet and Hess, 1986). Briefly, the test consists of pumping from EBR-4 at the indicated flow rate, and observing water levels in adjacent wells EBR-1, 2, and 3. A sensitive flowmeter was used in all the wells to establish horizons of inflow and outflow. In the table, the largest and smallest observed flow rates are reported.

ZERO OFFSET GEOMETRY
$\rho = 2700$ kg/m^3 $\alpha = 5.8$ km/s $\beta = 3.3$ km/s
$|\varepsilon| = 10^{-6}$ cm/cm
$\gamma = 5 \times 10^{-10}$ Pa^{-1}

	κL_0	$\lvert(D_1/D_4)(\partial P/\partial t)\rvert$	$\lvert(D_2/D_4)(\partial P/\partial t)\rvert$	$\lvert(D_3/D_4)(\partial P/\partial t)\rvert$
$f = 100$ Hz	2×10^9	2.0	4.9×10^{-5}	4.9×10^{-5}
	5×10^9	3.5		
$u(t) = 10\mu$m	10^{10}	11.0		
	2×10^{10}	12.3		
P_ζ =156 nt·m·sec	5×10^{10}	26.0		
$f = 200$ Hz	2×10^9	2.0	4.9×10^{-5}	4.9×10^{-5}
	5×10^9	3.5		
$u(t) = 5\mu$m	10^{10}	11.0		
	2×10^{10}	12.3		
P_ζ =78 nt·m·sec	5×10^{10}	26.0		
$f = 400$ Hz	2×10^9	2.0	3.9×10^{-5}	3.9×10^{-5}
	5×10^9	3.5		
$u(t) = 2\mu$m	10^{10}	11.0		
	2×10^{10}	12.3		
P_ζ =31 nt·m·sec	5×10^{10}	26.0		

Table A1: Parameter Study of Model Coefficients.

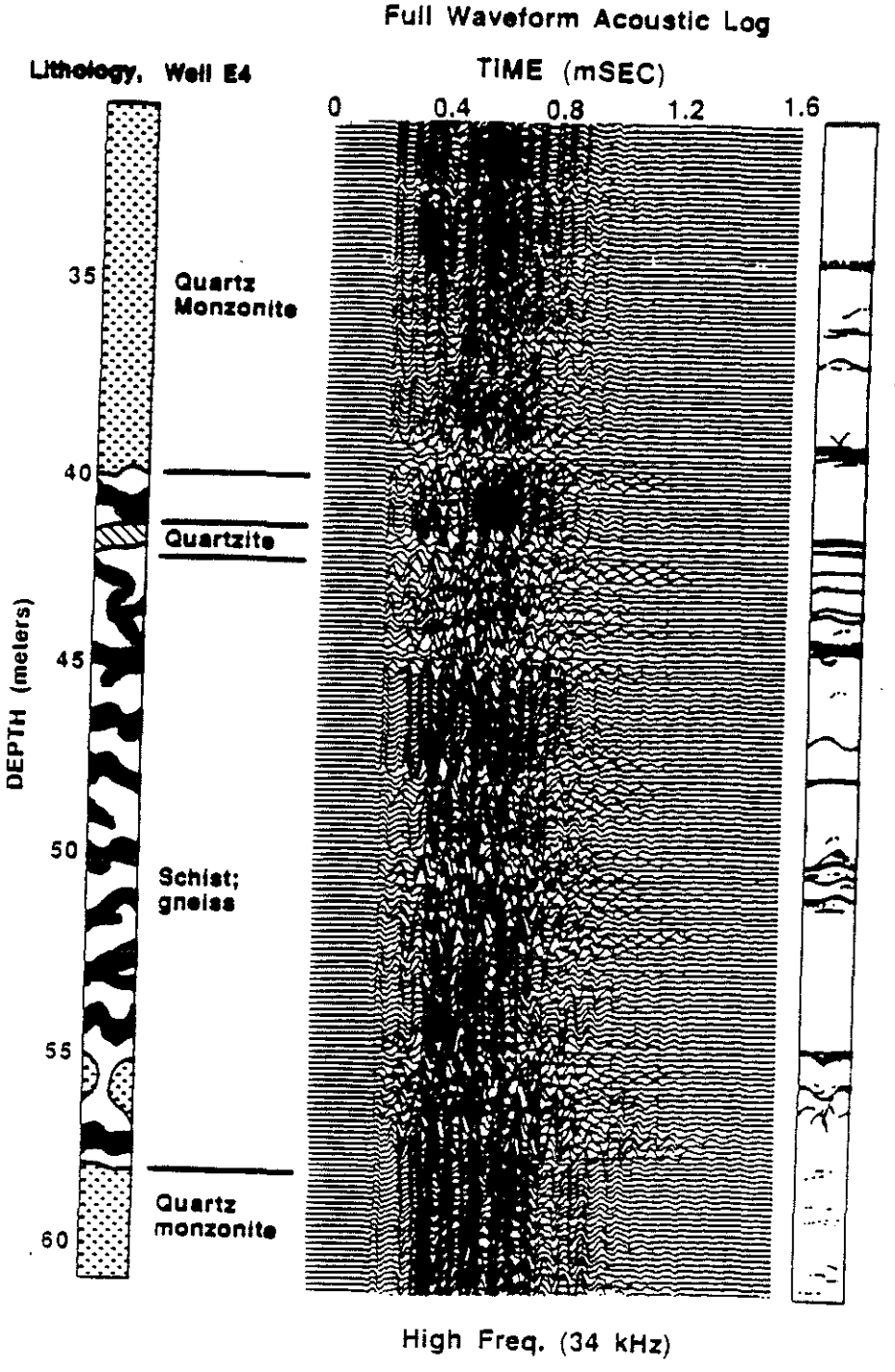

Figure 1: Full waveform acoustic log from EBR-4 Mirror Lake well, interval from 30 to 60 meters containing tube wave generating horizon at 44 meters. Separation: 0.91 meters, approx. source band center frequency: 34 kHz. Stoneley wave is nearly indistinguishable from the pseudo-Rayleigh modes.

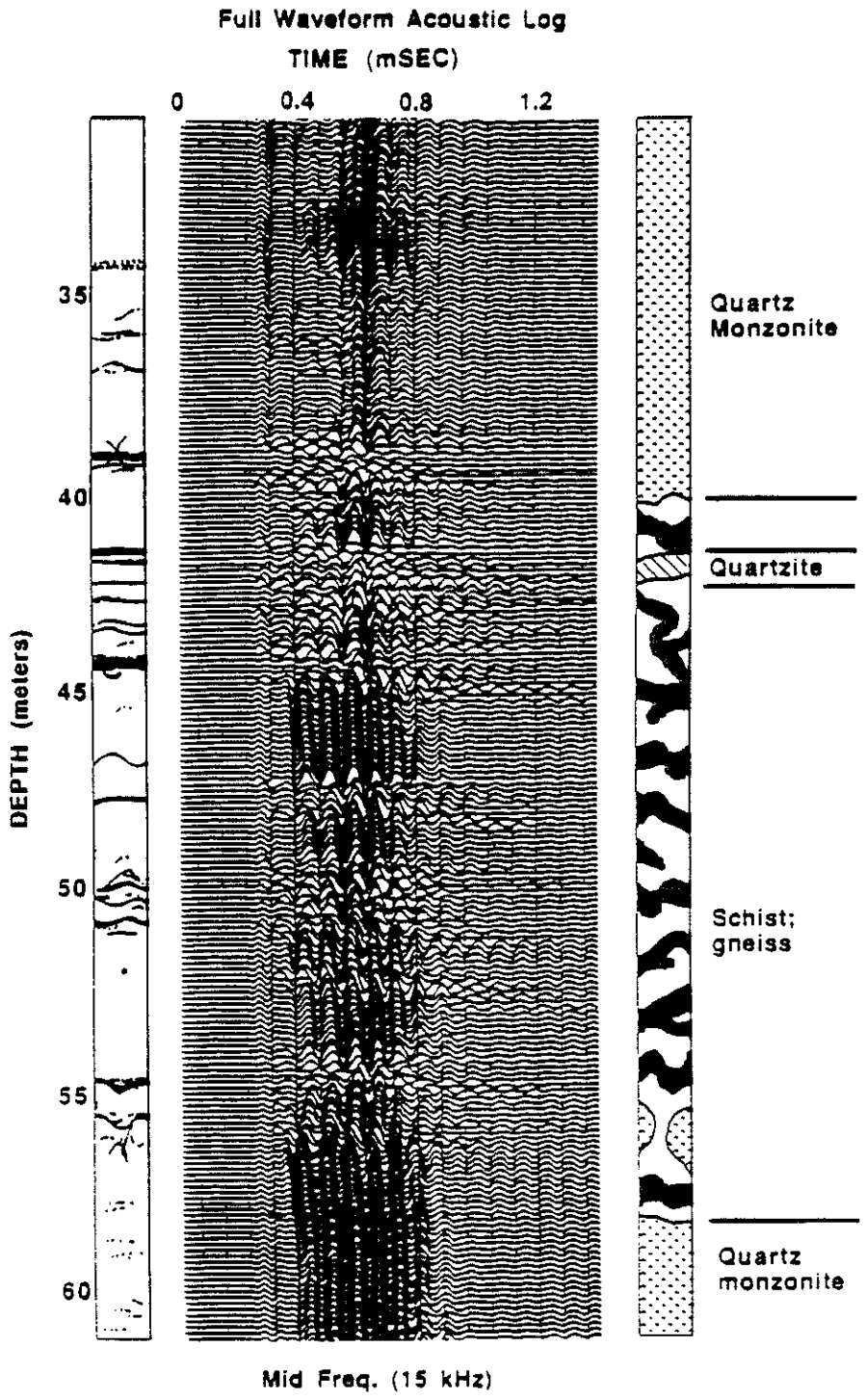

Figure 2: Full waveform acoustic log from EBR-4 Mirror Lake well, interval from 30 to 60 meters containing tube wave generating horizon at 44 meters. Separation: 0.91 meters, approx. source band center frequency: 15 kHz. Stoneley packet can be distinguished from pseudo-Rayleigh, although not at every depth.

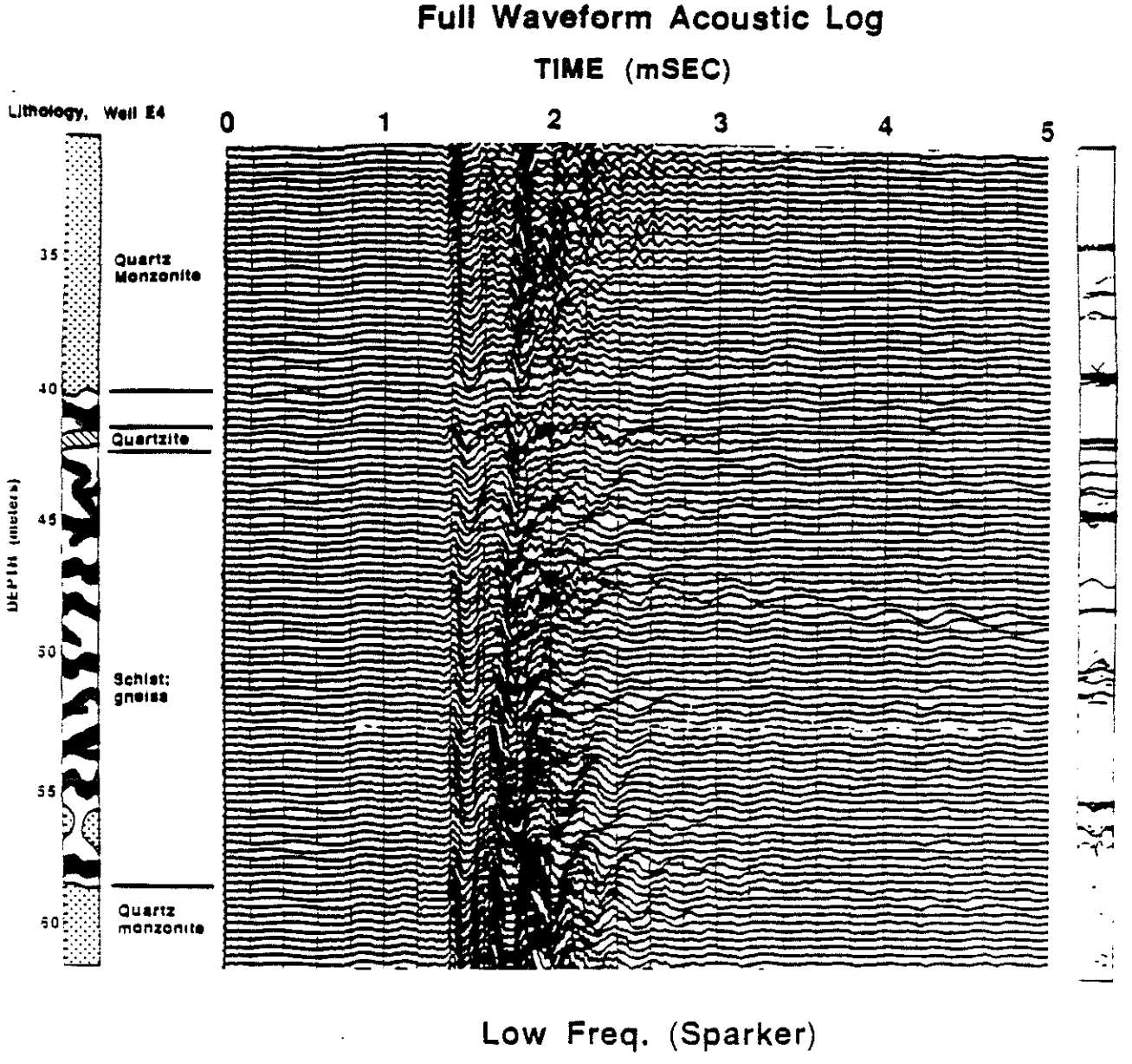

Figure 3: Full waveform acoustic log from EBR-4 Mirror Lake well, interval from 30 to 60 meters containing tube wave generating horizon at 44 meters. Separation 3.0 meters, approx. source band center frequency: 5 kHz. Pseudo-Rayleigh waves are not present since the source band is mostly below the cutoff frequency of the first mode.

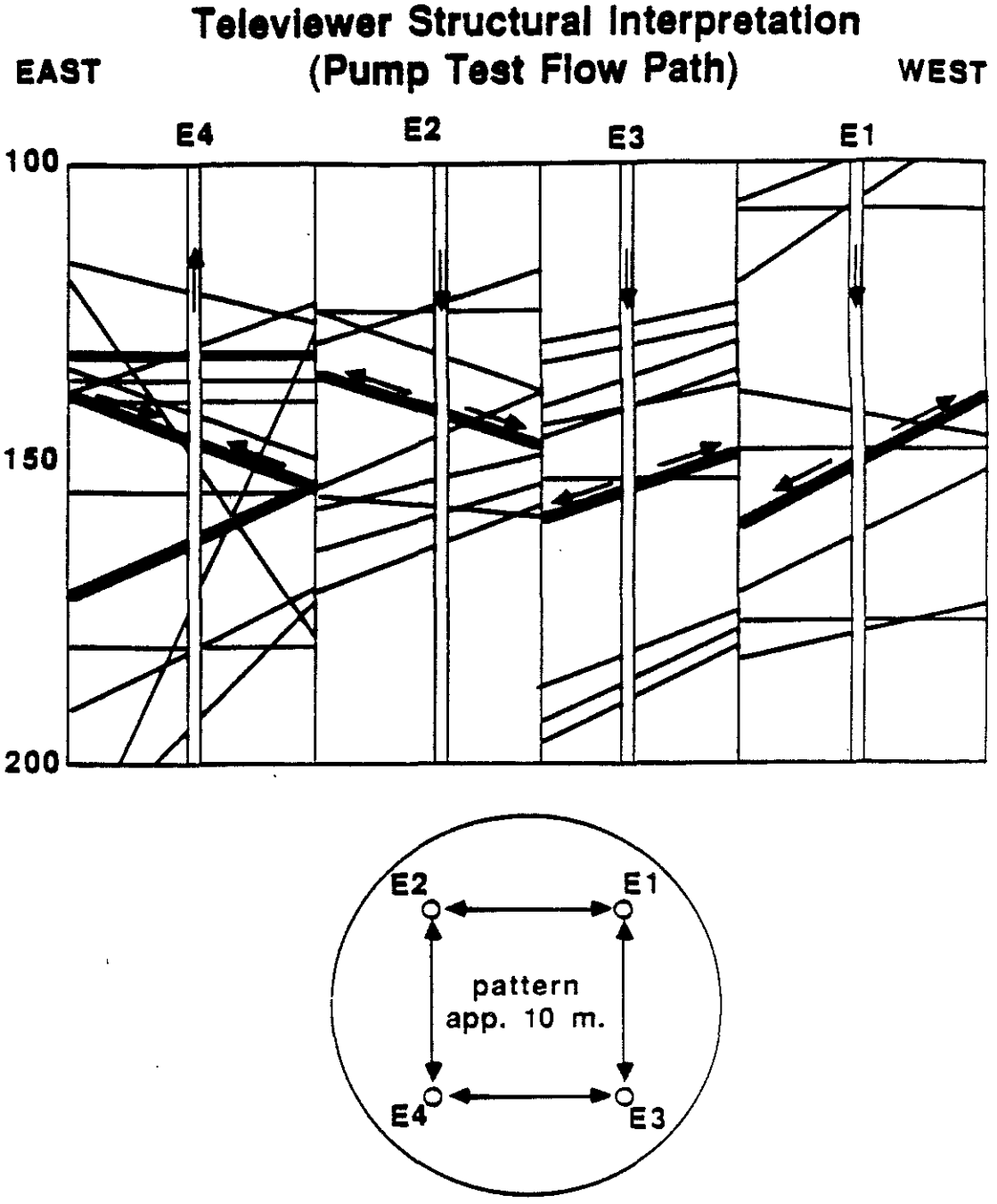

Figure 4: East-west cross-sections through wells EBR-1 thru -4, superposed to show possible flow paths. During discharge from EBR-4, all communicative flow in the other wells was observed near the depth of inflow into EBR-4.

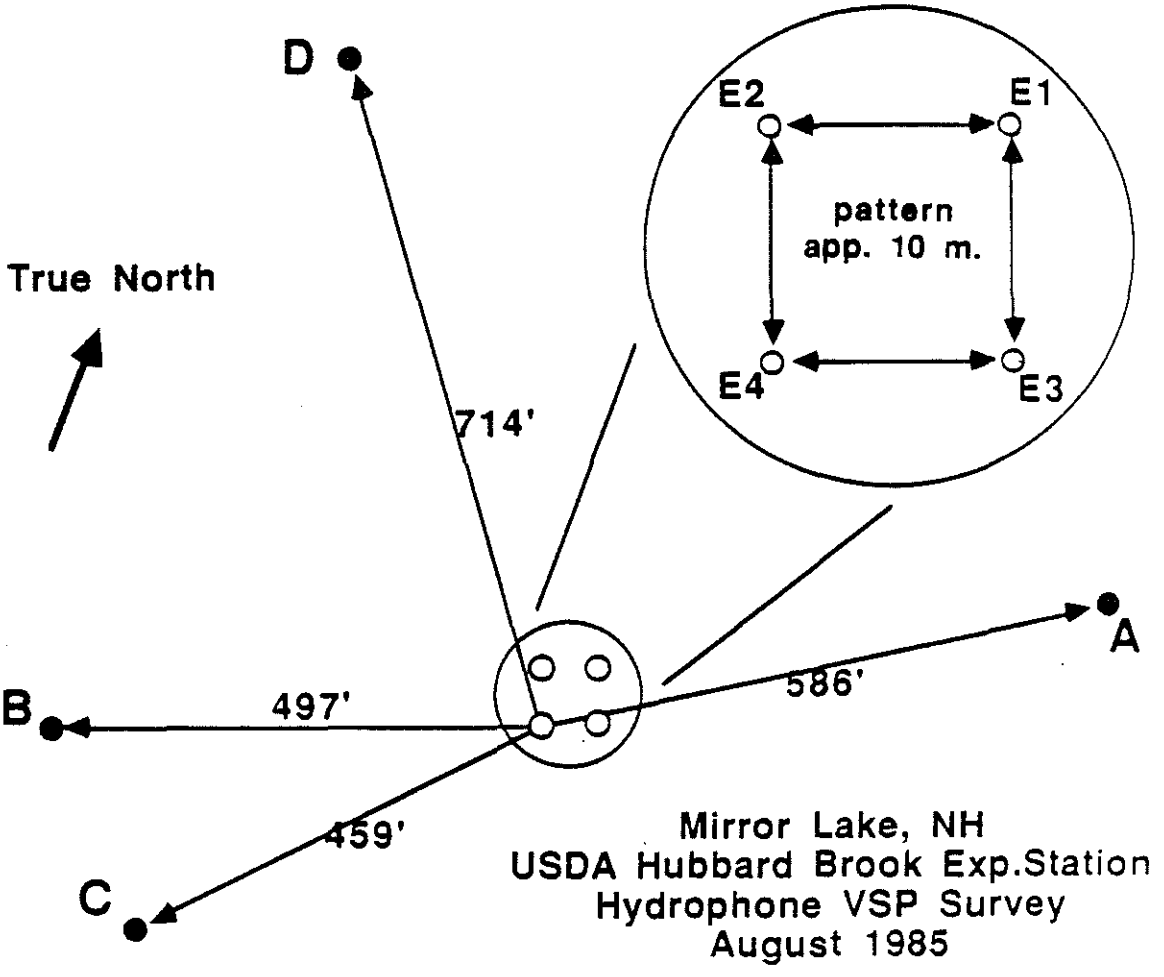

Figure 5: Schematic of VSP geometry at Mirror Lake site. Generated tube waves were observed in well EBR-4, by a string of hydrophones which could be moved up- and downhole. Timing and monitor phone signals were conveyed from distant shot holes A thru D, to recording equipment at EBR-4, by means of a multi-conductor surface cable.

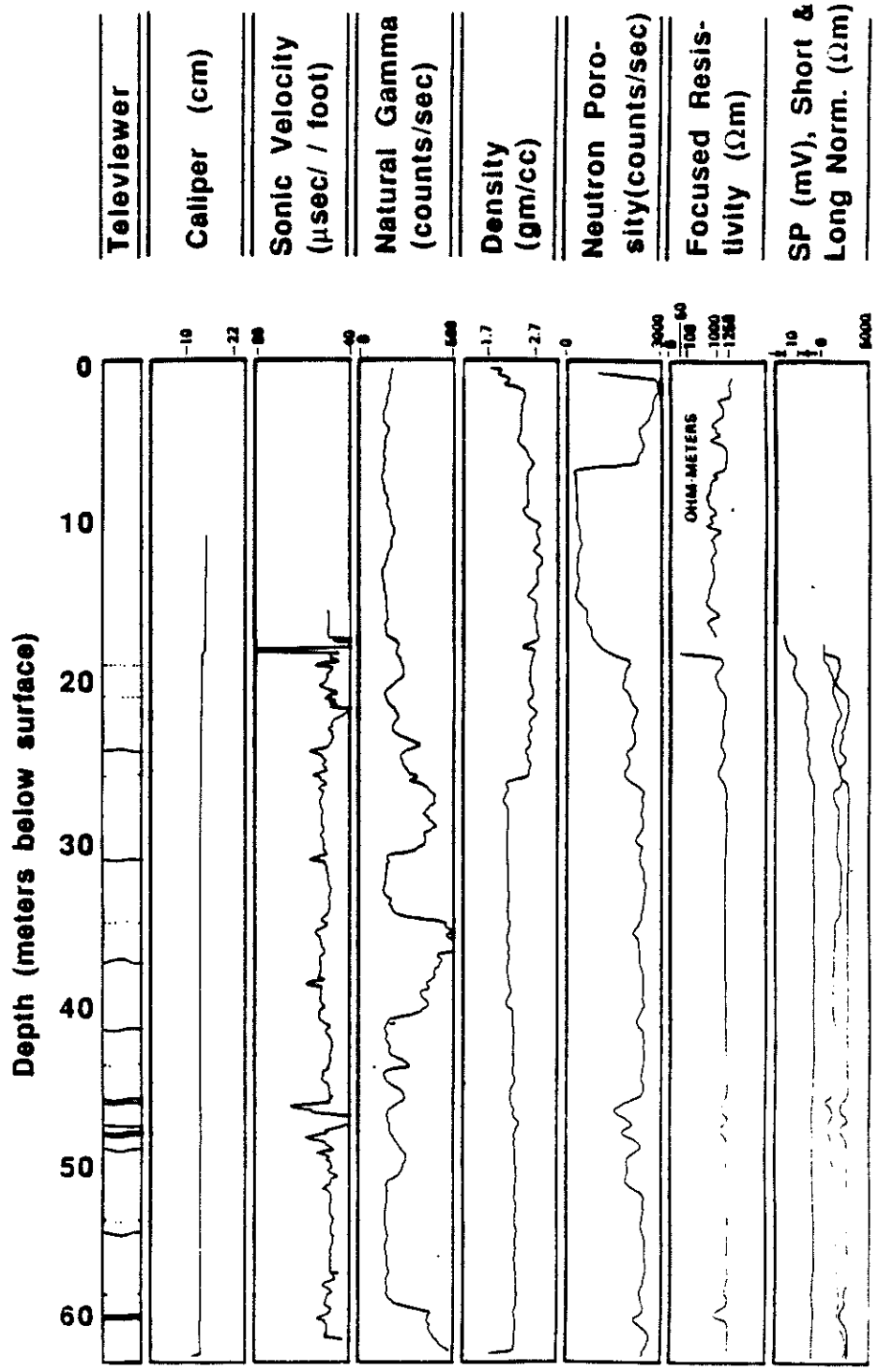

Figure 6: Wireline logs from Mirror Lake EBR-3, adjacent to observation well EBR-4. Artist's synopsis of televiewer images plotted for comparison (after Winters, 1984).

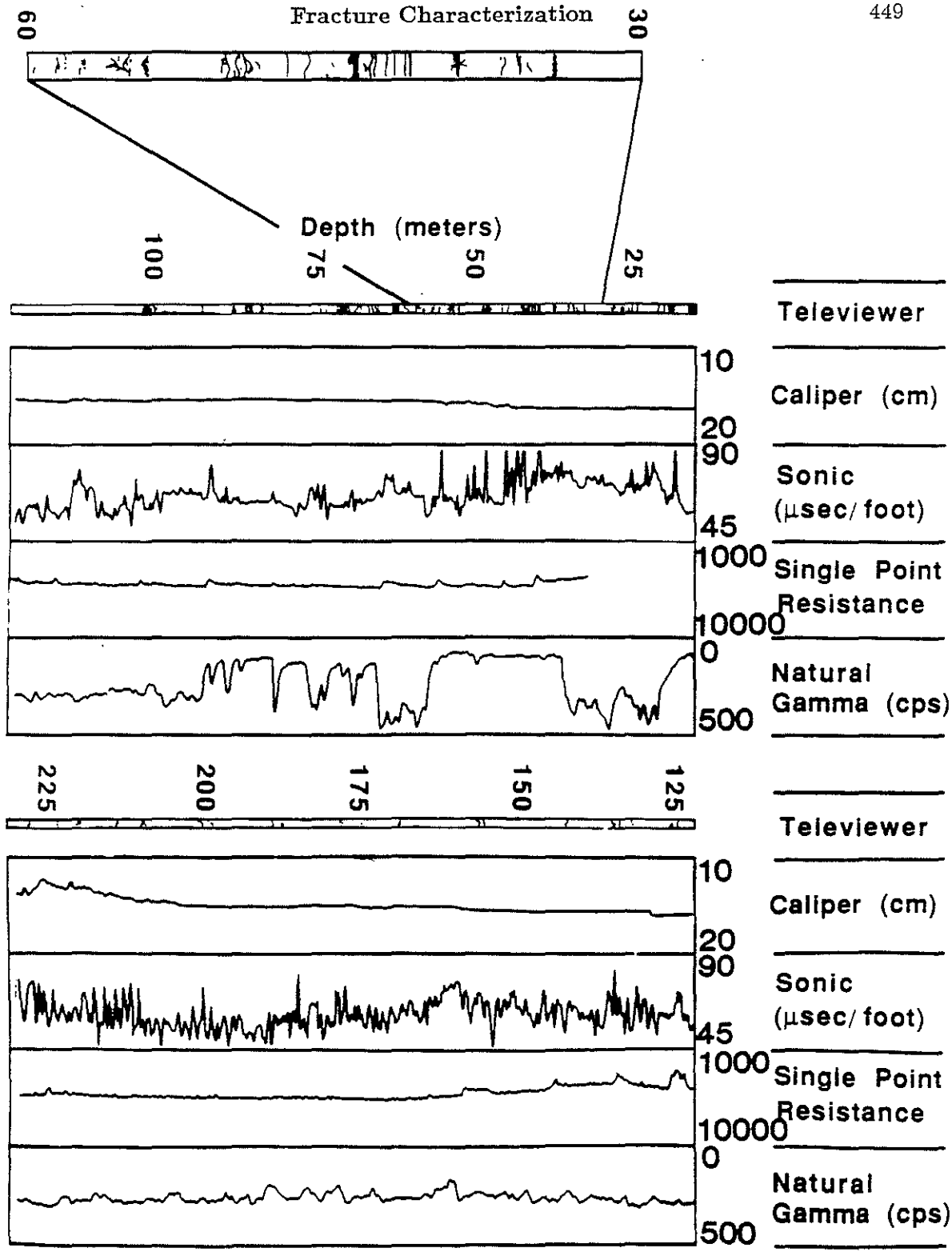

Figure 7: Wireline logs from Mirror Lake EBR-4. Artist's synopsis of televiewer images plotted for comparison (after Paillet, 1985).

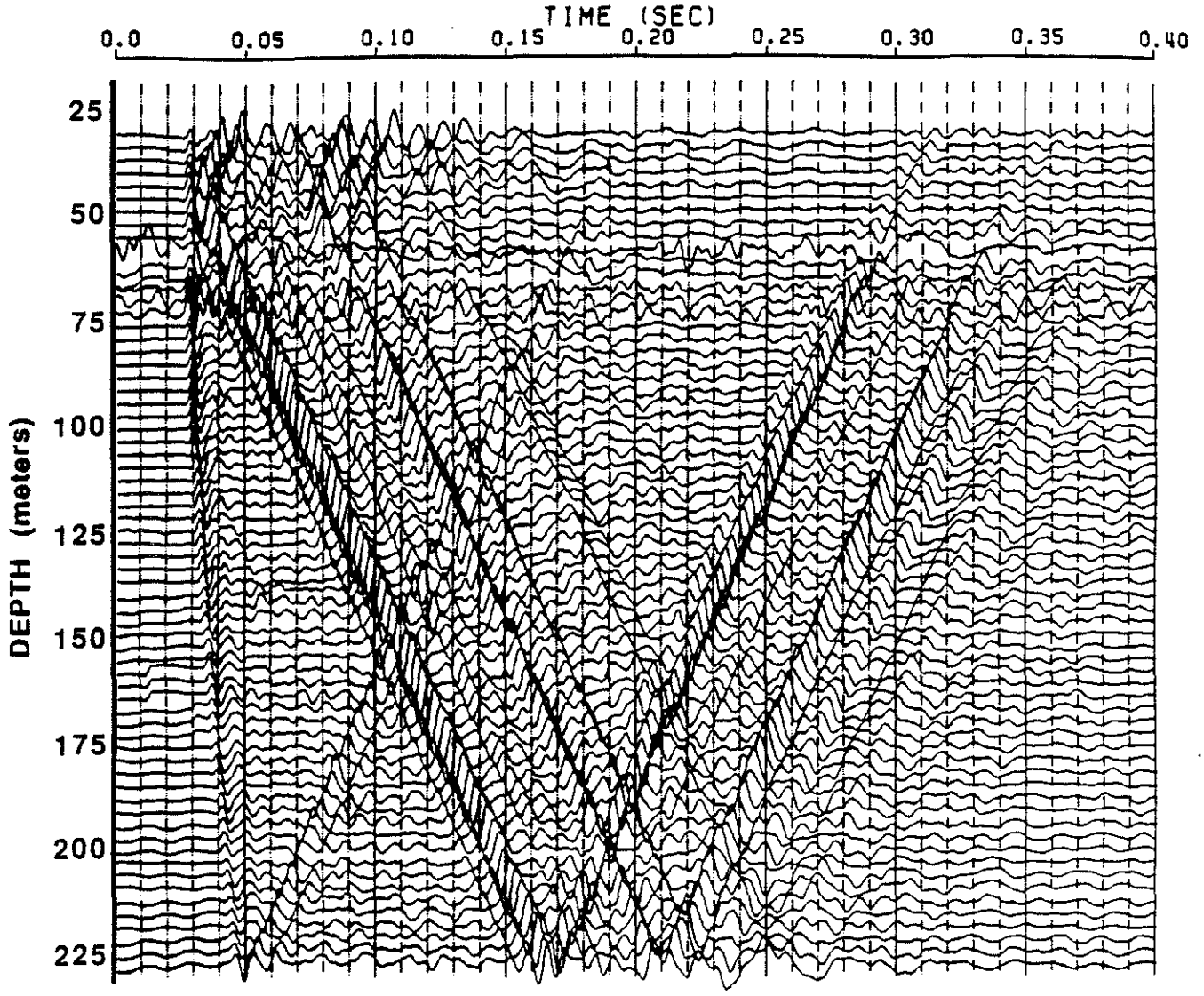

Figure 8: Hydrophone VSP section from Mirror Lake experiment, observation well EBR-4, shot hole A. Traces are bandpass filtered (100-300 Hz.) and shifted to zero-time defined by the monitor phone break.

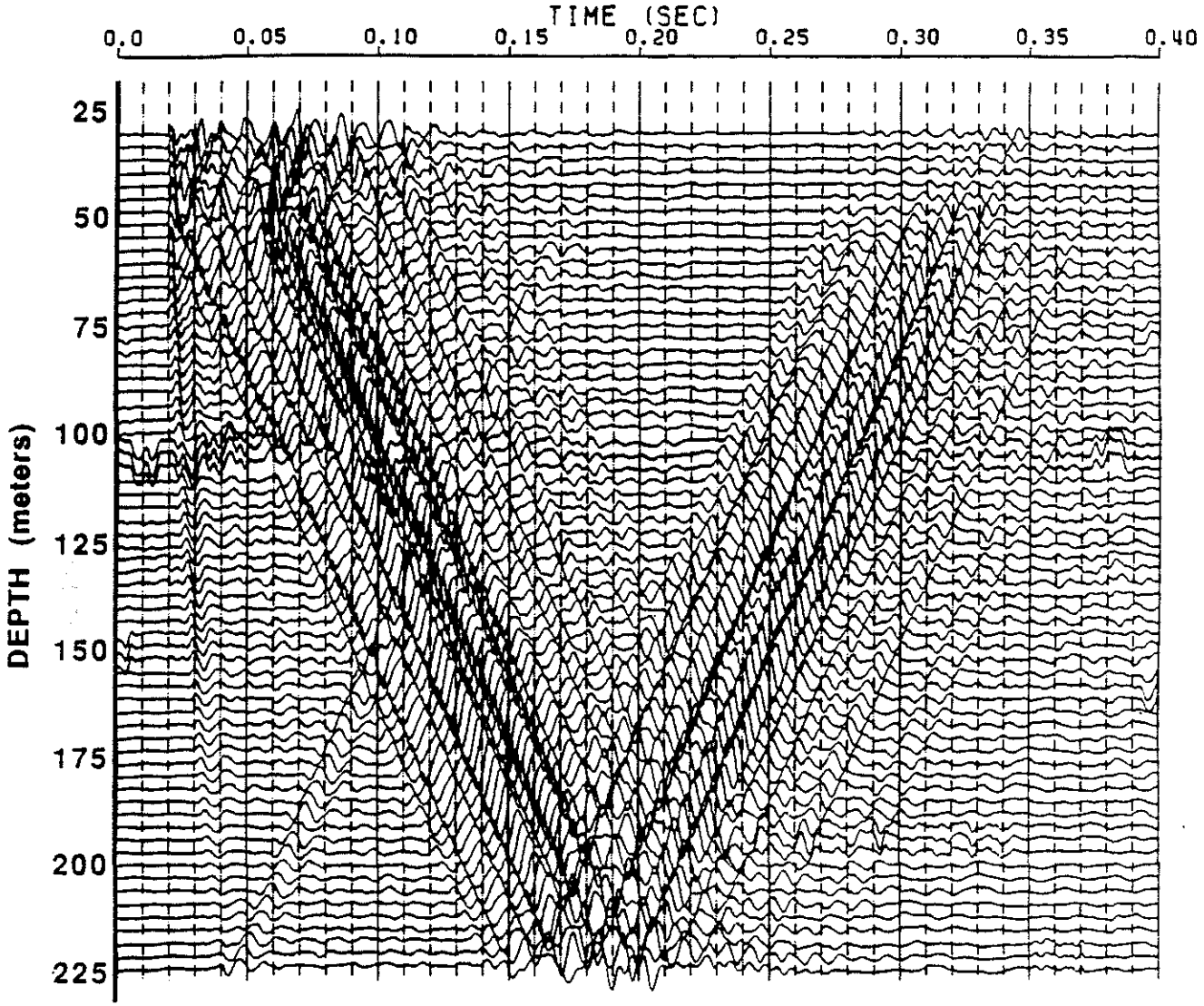

Figure 9: Hydrophone VSP section from Mirror Lake experiment, observation well EBR-4, shot hole B. Traces are bandpass filtered (100-300 Hz.) and shifted to zero-time defined by the monitor phone break.

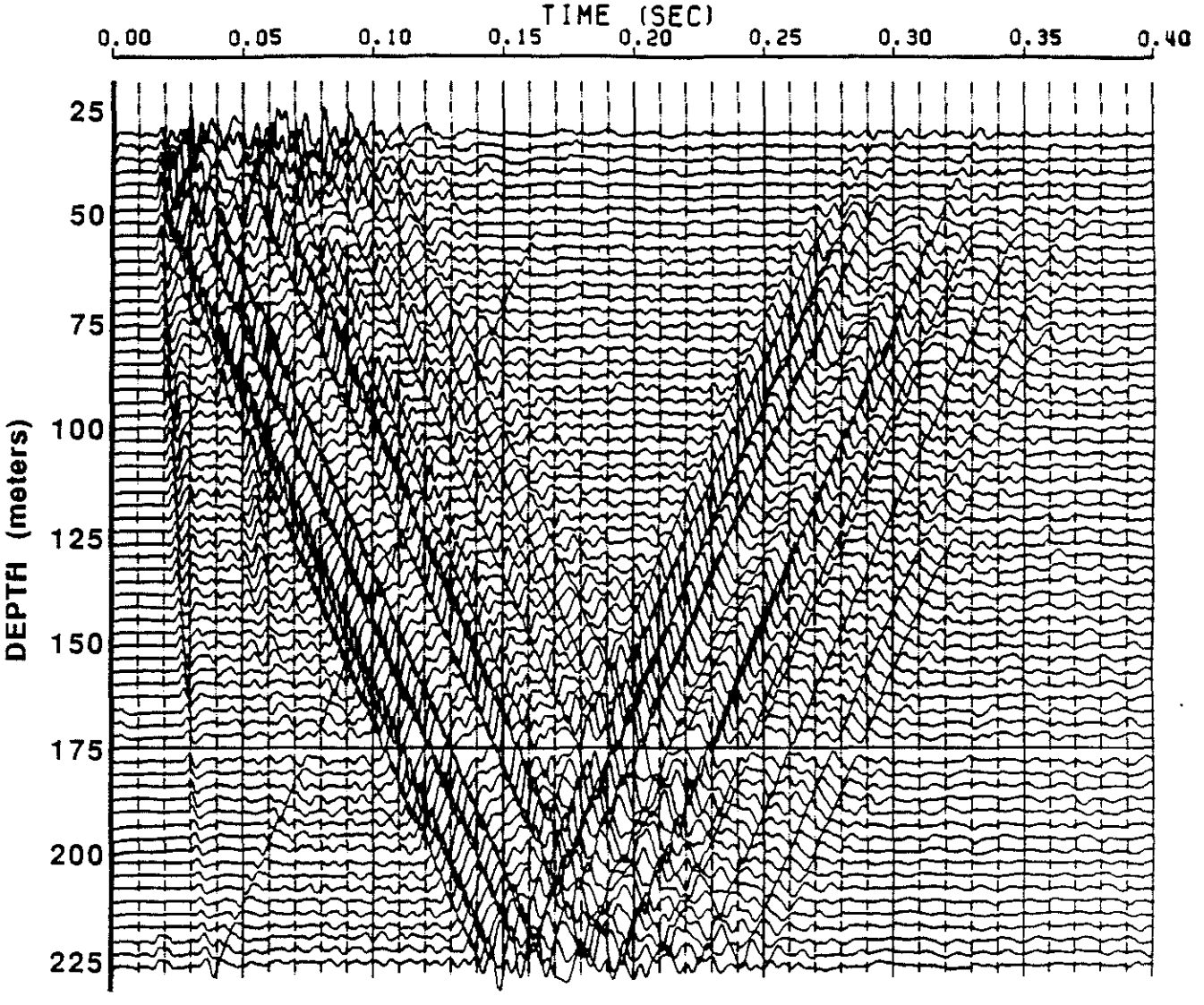

Figure 10: Hydrophone VSP section from Mirror Lake experiment, observation well EBR-4, shot hole C. Traces are bandpass filtered (100-300 Hz.) and shifted to zero-time defined by the monitor phone break.

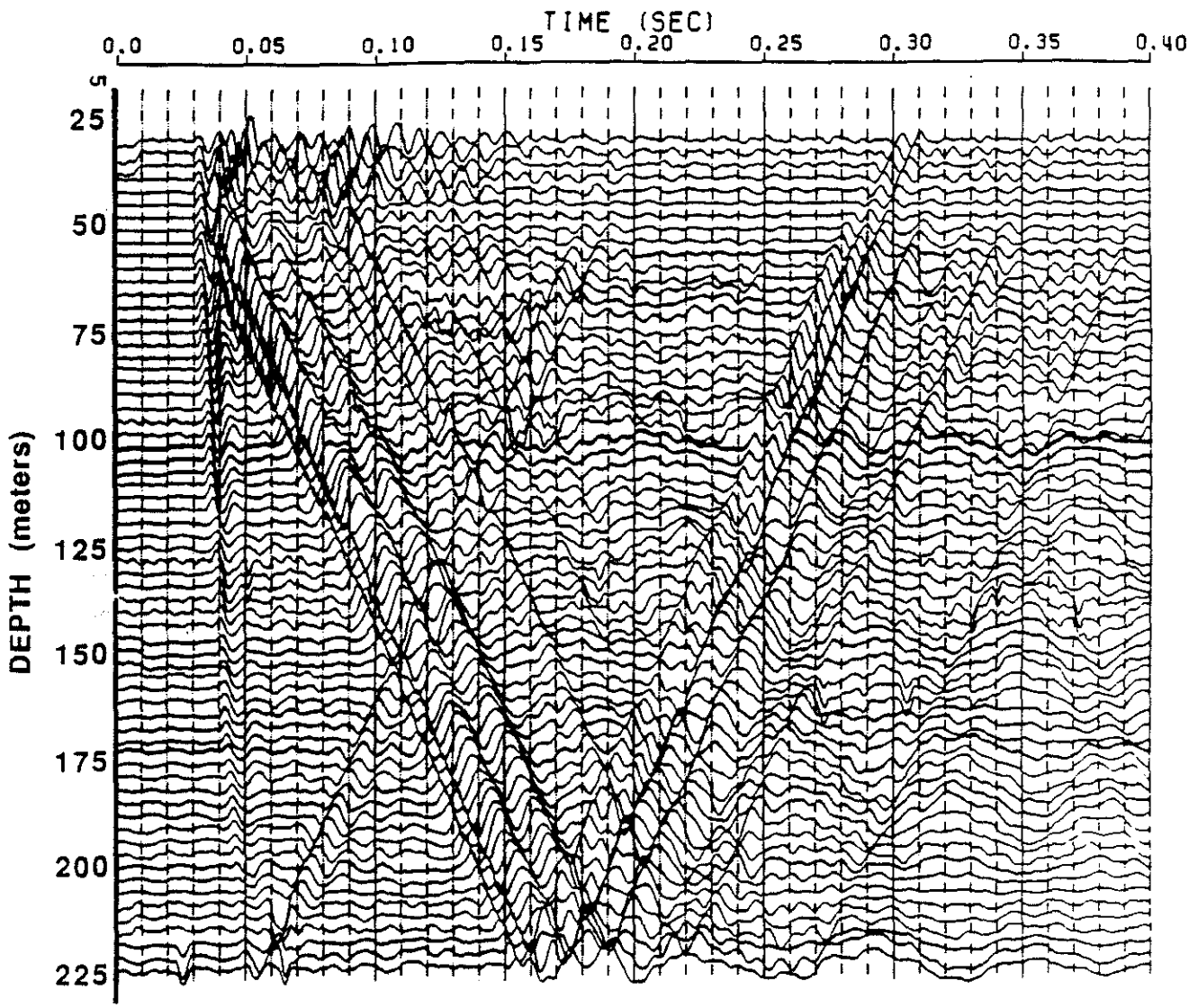

Figure 11: Hydrophone VSP section from Mirror Lake experiment, observation well EBR-4, shot hole D. Traces are bandpass filtered (100-300 Hz.) and shifted to zero-time defined by the monitor phone break.

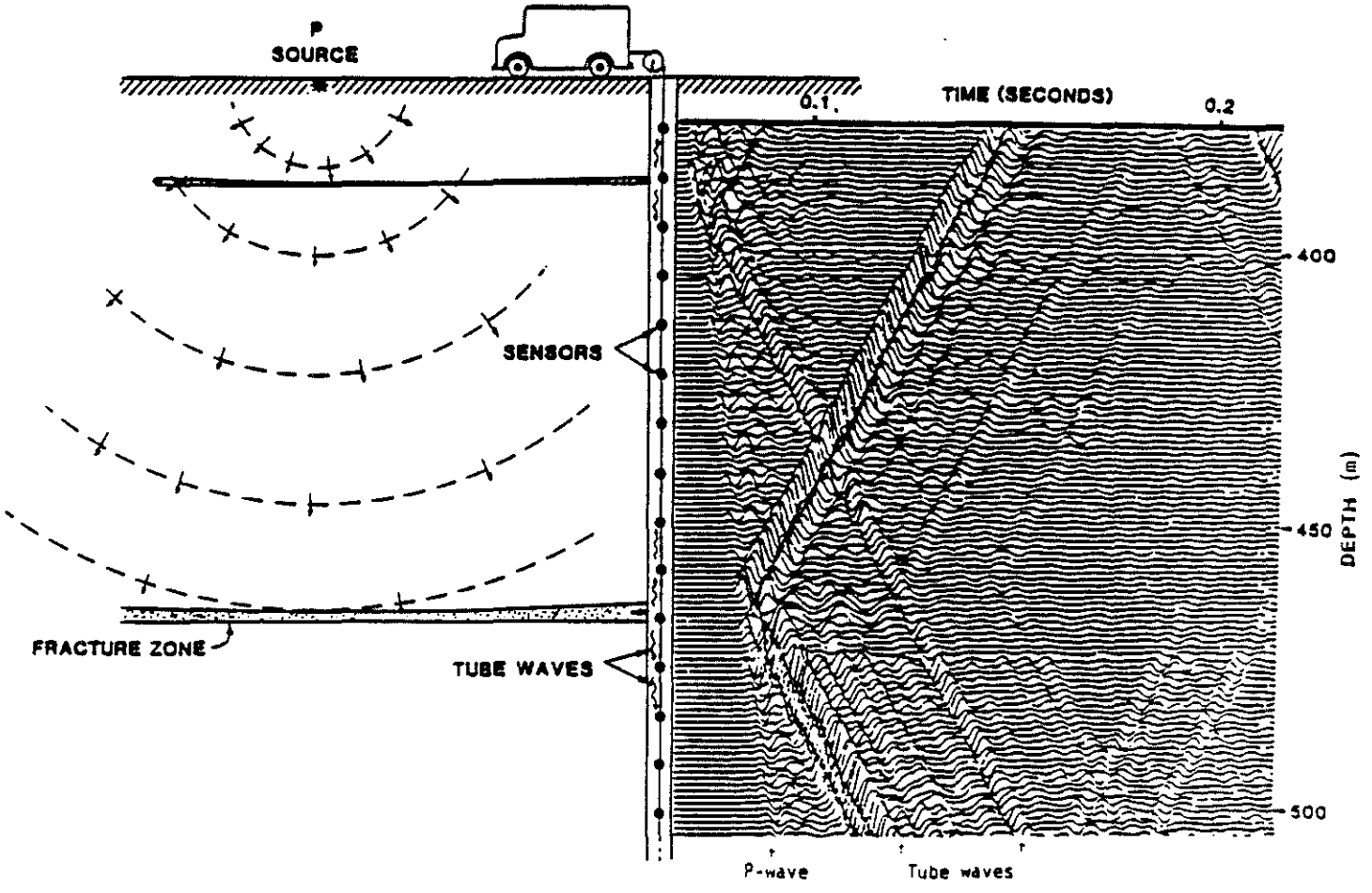

Figure 12: VSP generation mechanism schematic. A direct compressional wave interacts with the fracture, resulting in mass transfer to the borehole and a generated tube wave.

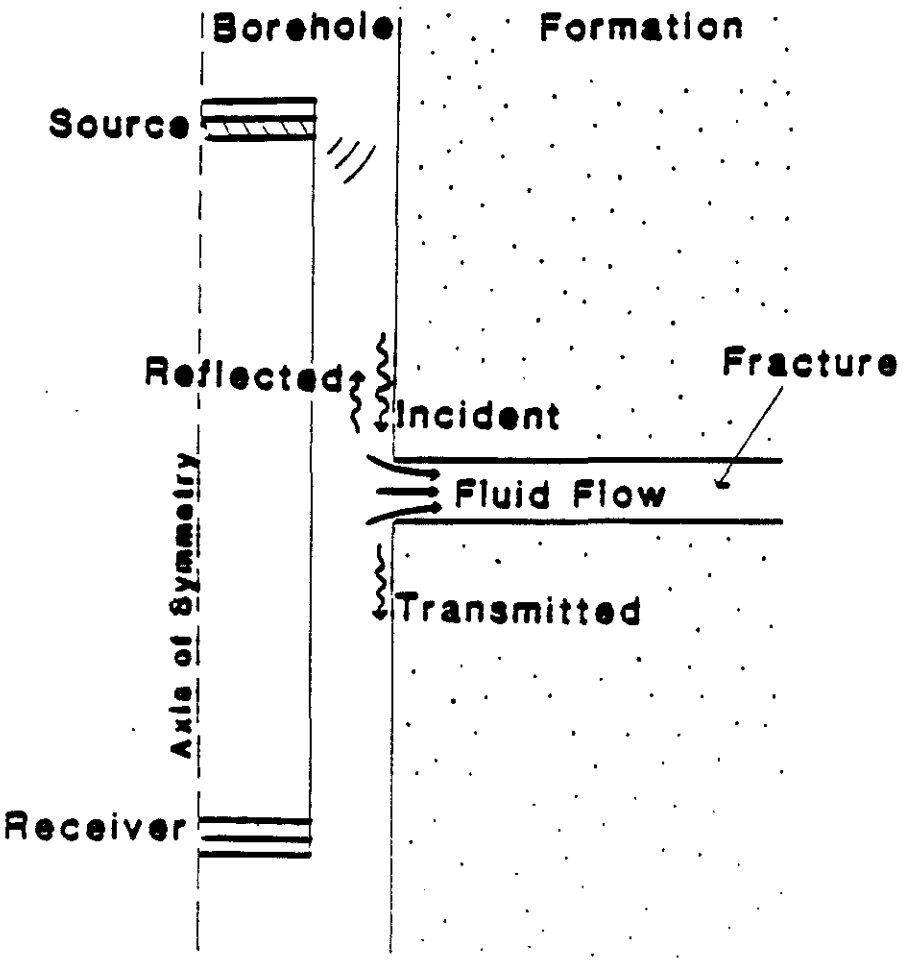

Figure 13: Schematic of FWAL Stoneley phase attenuation mechanism. Dynamic pressure at the opening of the fracture into the borehole is the sum of pressure signals due to fracture flow, and incident/reflected/transmitted Stoneley waves.

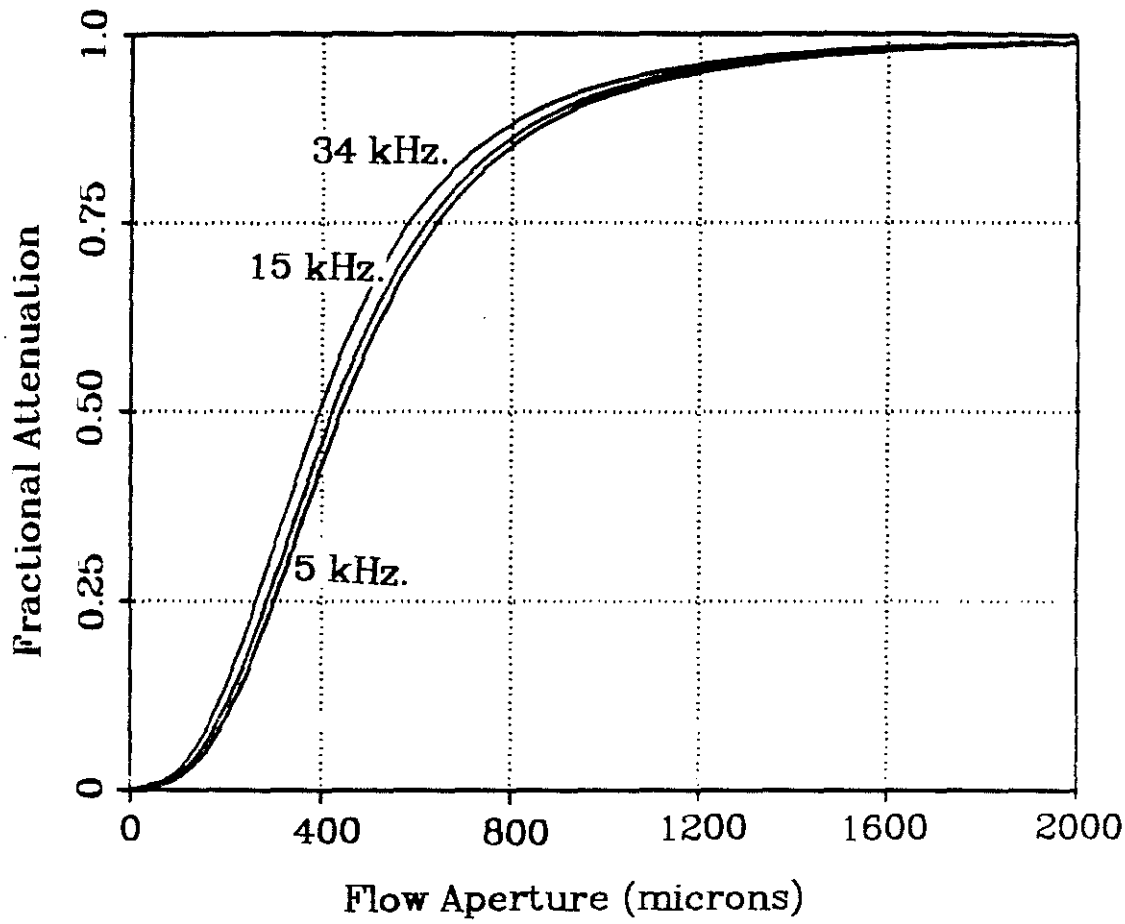

Figure 14: Fractional Stoneley attenuation (ratio of far:near receivers) vs. fracture flow-aperture. Different curves correspond to different frequencies as indicated.

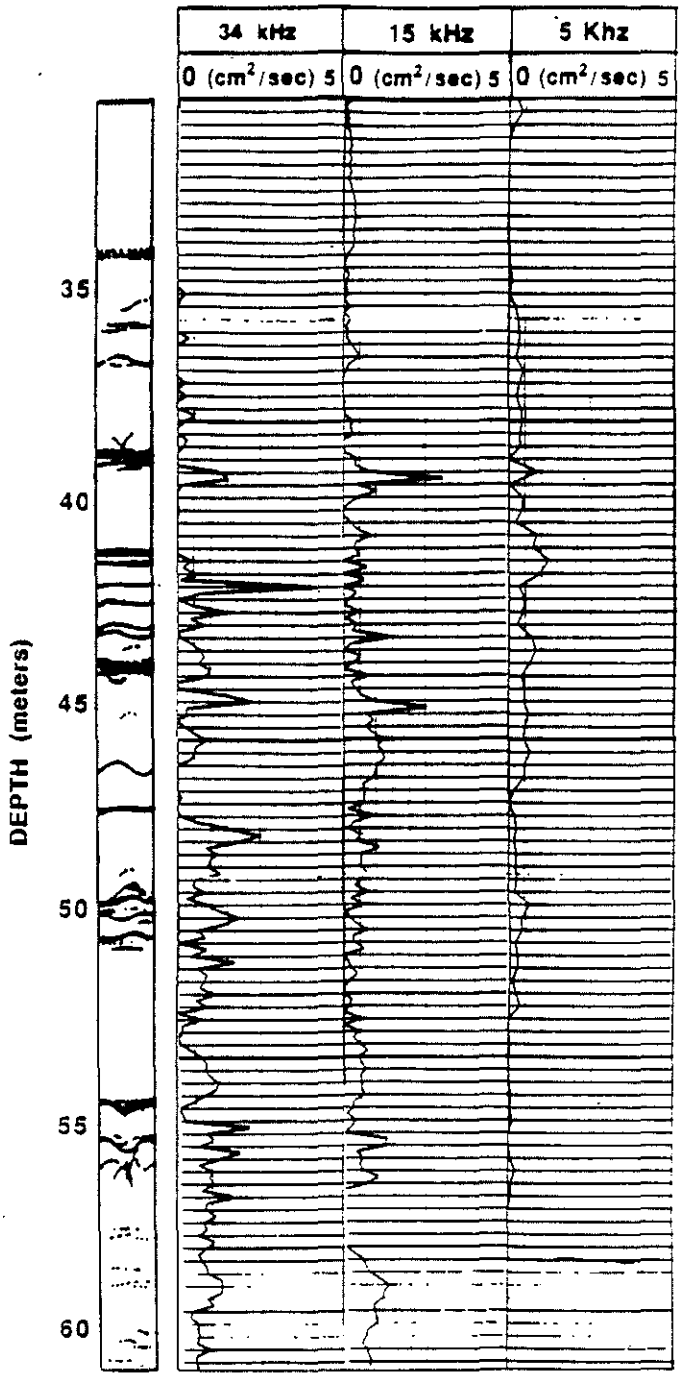

Figure 15: Calculated transmissivity vs. depth, from FWAL Stoneley attenuation.
(a) Tx/Rx separations: 0.6 and 0.91 meters., 34 kHz. magnetostrictive source
(b) Tx/Rx separations: 0.6 and 0.91 meters., 15 kHz. magnetostrictive source
(c) Tx/Rx separations: 2.1 and 3.0 meters., 5 kHz., sparker source.

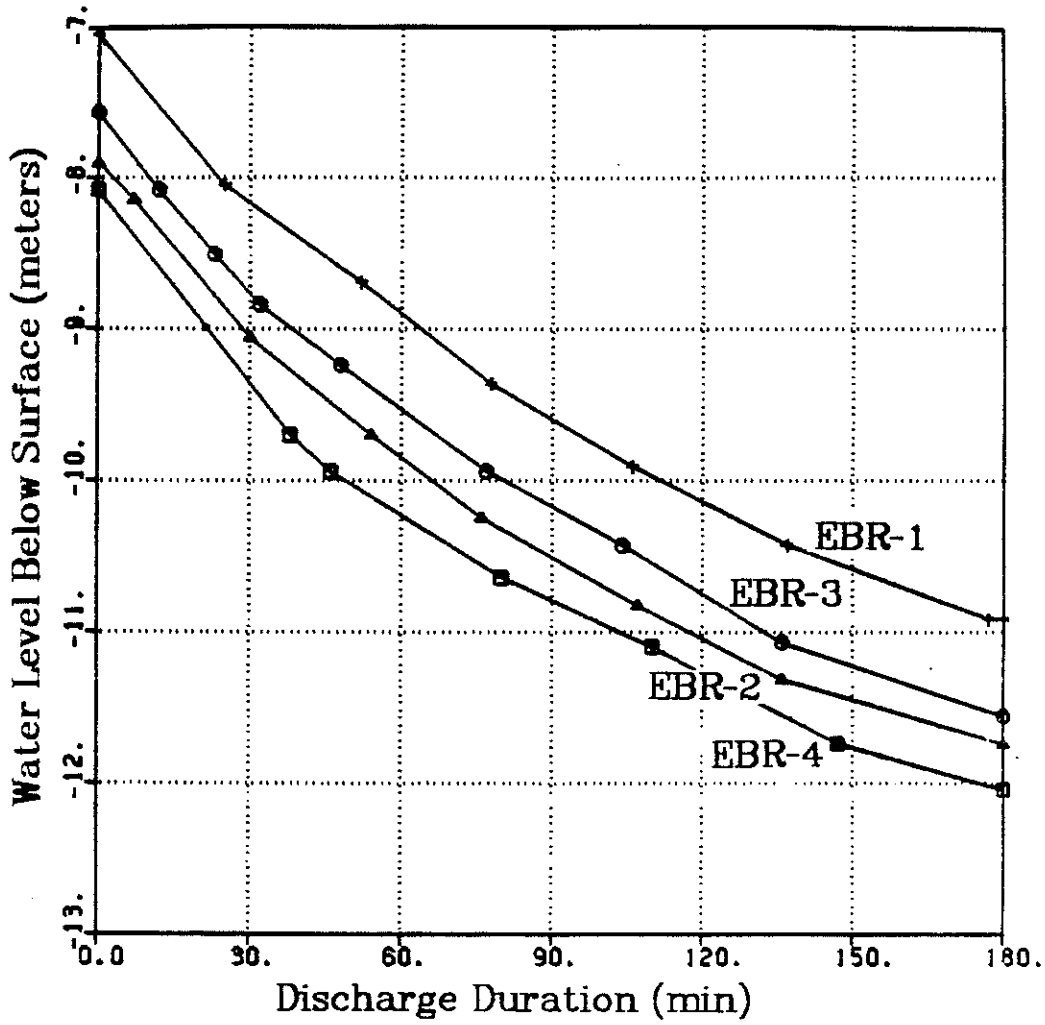

Figure 16: Head fall in wells EBR-1,2 and 3 vs. time, during EBR-4 constant discharge pump test (after Paillet). EBR-4 is the pumped well.

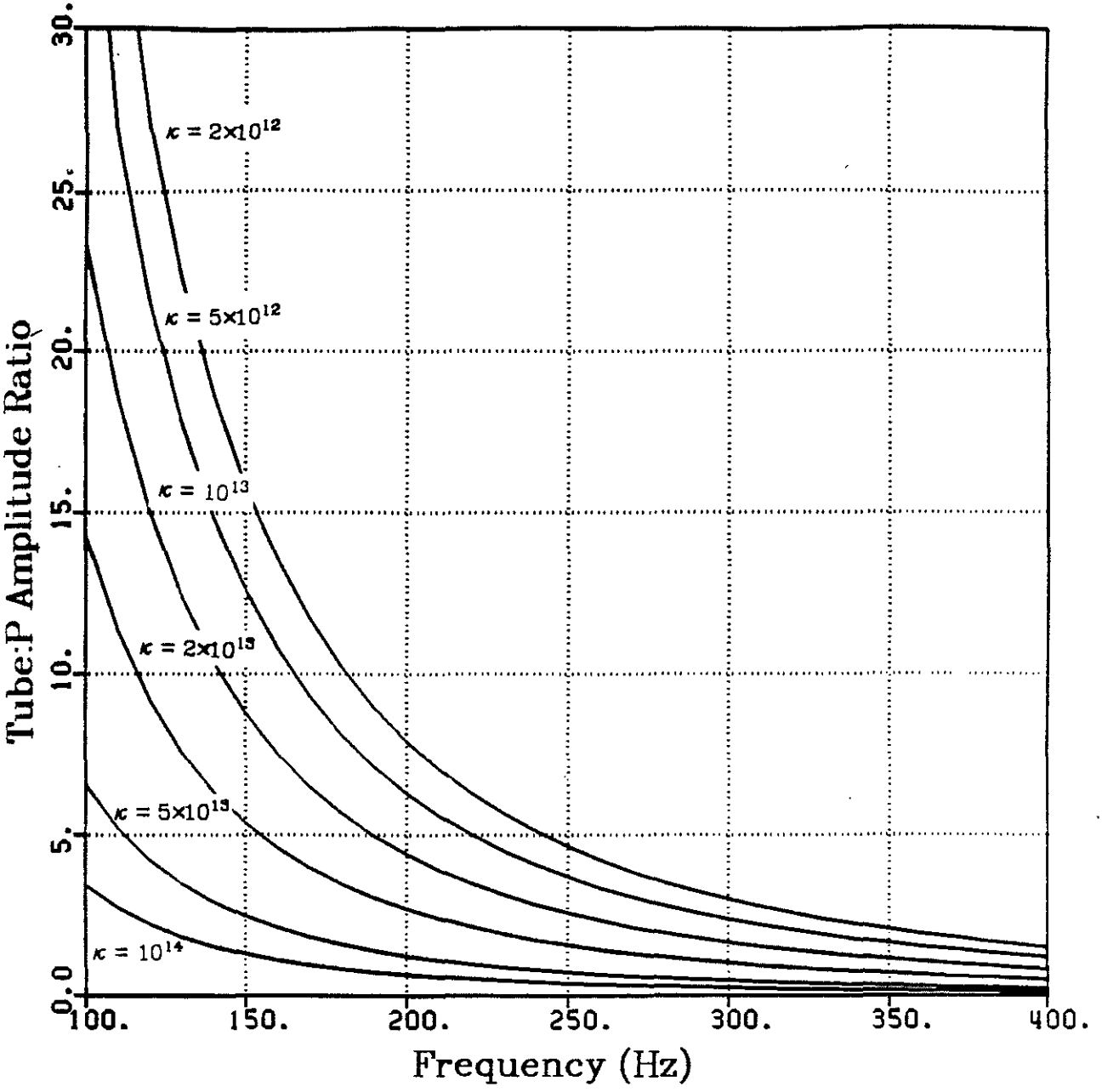

Figure 17: Tube:P amplitude ratio vs. frequency, from stress formulation, using zero offset, normal incidence geometery, and parameters appropriate to well EBR-4 (fracture at 44 m). Different curves correspond to different values of fracture stiffness, as indicated.

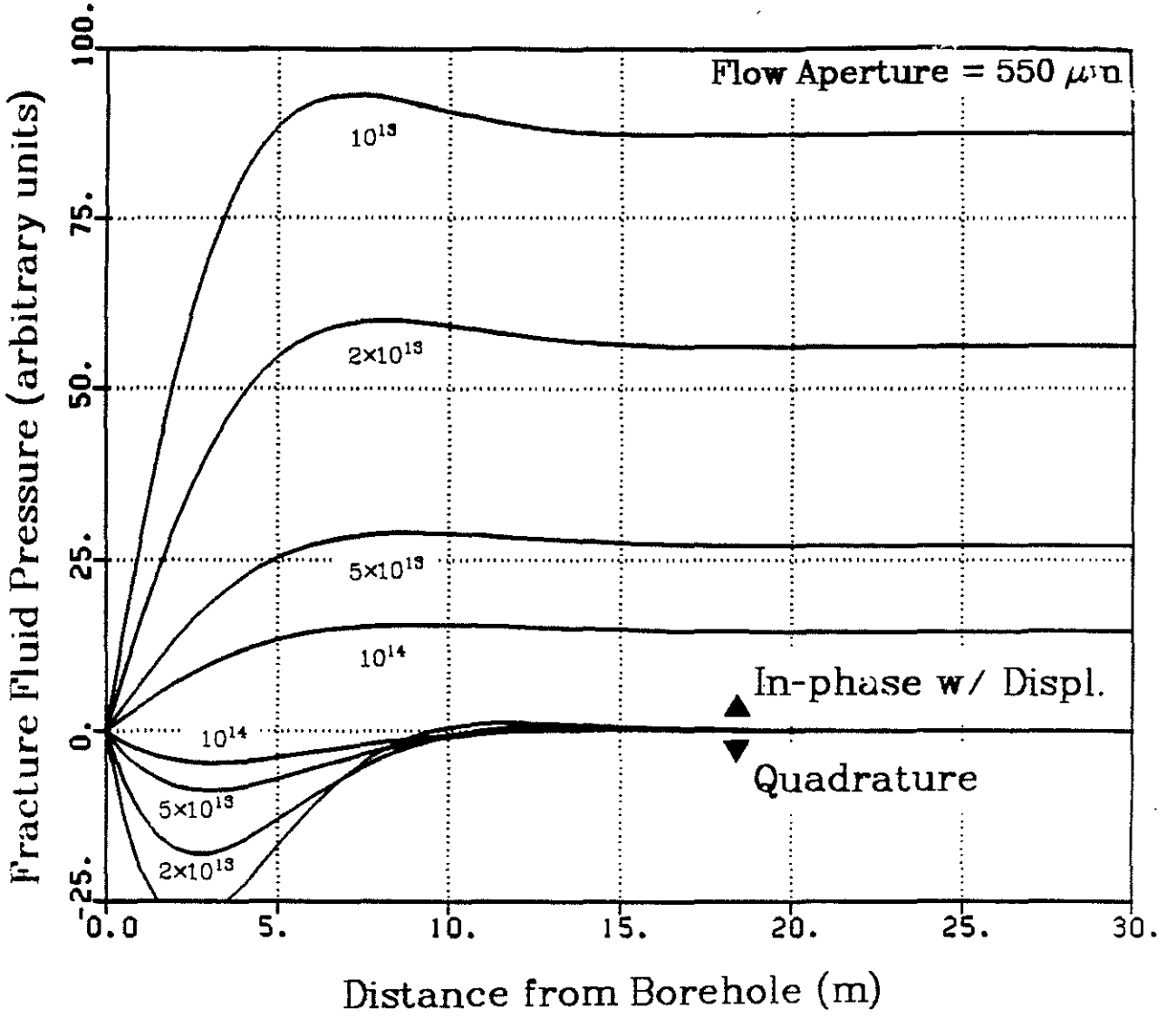

Figure 18: Dynamic 2-D pressure transfer function for stress formulation. Real and imaginary components are plotted for several values of fracture stiffness.